

FORMULATION OF PERFLUOROCARBON-FILLED DROPLETS FOR
ULTRASOUND-MEDIATED APPLICATIONS

by

Vincent Wong

Copyright © Vincent Wong 2011

A Thesis Submitted to the Faculty of the
BIOMEDICAL ENGINEERING GRADUATE INTERDISCIPLINARY PROGRAM

In Partial Fulfillment of the Requirements
For the Degree of

MASTER OF SCIENCE
WITH A MAJOR IN BIOMEDICAL ENGINEERING

THE UNIVERSITY OF ARIZONA

2011

In the Graduate College

STATEMENT BY AUTHOR

This thesis has been submitted in partial fulfillment of requirements for an advanced degree at the University of Arizona and is deposited in the University Library to be made available to borrowers under rules of the Library.

Brief quotations from this thesis are allowable without special permission, provided that accurate acknowledgment of source is made. Requests for permission for extended quotation from or reproduction of this manuscript in whole or in part may be granted by the copyright holder.

SIGNED: *Terrill Way*

APPROVAL BY THESIS DIRECTOR

This thesis has been approved on the date shown below:

Terry O. Matsunaga
Terry O. Matsunaga
Radiology Research Professor

05/19/2011
Date

ACKNOWLEDGEMENTS

First and foremost, I would like to thank Dr. Terry Matsunaga for taking the risk of taking me under his wing to learn from him. I am indebted to him and his family for their moral support for both my academic and personal life.

Thanks to the rest of the Matsunaga research team for putting up with me and maintaining the excitement in this research: Shannon Degrote for teaching me how to make liposomes; Kyle McKeown for teaching me how to make microbubbles; Alice Ferng for showing me how to approach things more scientifically; Ryan McFarland for his reassurance; Erin Ogram for preparing excess lipid films; and Dr. Bill Ross for his proactive efforts.

I would also like to thank the following people for their assistance in this project: Dr. Josef Vagner for permitting use of a lyophilizer; the entire team at University Spectroscopy and Imaging Facilities (USIF) at the University of Arizona, especially David Bentley for teaching me how to prepare samples for transmission electron microscopy; Dr. Supapan Seraphin for teaching me about the physics involved in transmission electron microscopy; the University of Arizona Cryogenics & Gas Facility; Dr. Brigitte Papahadjopoulos-Sternberg for her assistance with freeze-fracture electron microscopy; Dr. Samuel Yalkowsky for permitting use of a particle size analyzer; and last but not least, Dr. Paul Dayton's laboratory team at the Joint Department of Biomedical Engineering at the University of North Carolina, especially Paul Sheeran for accomplishing and polishing a much improved setup for acoustic droplet vaporization experiments.

DEDICATION

To my children, Meiling Lily-Rose Wong and Mingli Jon-George Wong.

TABLE OF CONTENTS

LIST OF FIGURES.....	7
LIST OF TABLES.....	9
ABSTRACT.....	10
1. INTRODUCTION AND LITERATURE REVIEW: DESIGN RATIONALE.....	11
1.1. Vascular Contrast Agents.....	14
1.2. Perfluorocarbons.....	17
1.3. Requirements for Vascular Diffusion.....	19
1.4. Requirements for Ultrasound-Mediated Vaporization.....	19
1.5. Potential Bioeffects.....	20
1.6. Design Proposal.....	22
1.7. Theory.....	26
1.8. Prior Works.....	29
1.9. Specific Aims and Hypotheses.....	30
2. MATERIALS AND METHODS.....	33
2.1. Preparation of Perfluorocarbon Droplets.....	33
2.2. Preparation of Perfluorobutane Droplets.....	34
2.3. Identification of Droplet Storage Stability.....	35
2.4. Scanning Electron Microscopy (SEM).....	36
2.5. Transmission Electron Microscopy (TEM).....	37
2.6. Freeze-Fracture TEM.....	37
2.7. Experimental Apparatus.....	38

TABLE OF CONTENTS - Continued

2.8.	Acoustics.....	40
3.	RESULTS.....	41
3.1.	Storage Stability.....	41
3.2.	Acoustic Droplet Vaporization (ADV).....	47
3.3.	Encapsulation of Perfluorobutane.....	50
4.	DISCUSSION.....	55
4.1.	Storage Stability of Perfluorocarbon Droplets.....	55
4.2.	Vaporization Thresholds of Perfluorocarbon Droplets.....	56
4.3.	Perfluorobutane Encapsulation.....	60
5.	CONCLUSIONS.....	61
5.1.	Conclusions on Storage Stability of Droplets.....	61
5.2.	Conclusions on Vaporization Thresholds.....	61
5.3.	Conclusions on Perfluorobutane Encapsulation.....	61
6.	FUTURE STUDIES.....	63
APPENDIX A:	SPREADSHEET OF PERFLUOROCARBON DROPLET CALCULATIONS.....	70
APPENDIX B:	CALCULATIONS FOR ESTIMATED VAPOR TEMPERATURES...	71
APPENDIX C:	DATA AND DATA ANALYSIS FOR STABILITY.....	74
APPENDIX D:	SEM IMAGE OF PFP DROPLETS.....	79
REFERENCES.....		80

LIST OF FIGURES

Figure 1.1: Microbubble with lipid shell and gaseous perfluorocarbon (PFC) core.....	16
Figure 1.2: Probubble design in initial and final states.....	22
Figure 1.3: Schematic of <i>in vivo</i> application of probubble precursor design.....	24
Figure 1.4: Estimated vapor temperature of perfluorocarbon within droplet.....	29
Figure 2.1: Experimental setup.....	39
Figure 3.1: Z-averages for nine samples that were stored at 4°C and monitored for 16 weeks.....	41
Figure 3.2: Z-averages for nine samples that were stored at 23°C and monitored for 16 weeks.....	42
Figure 3.3: Z-averages for nine samples that were stored at 40°C and monitored for 12 weeks.....	42
Figure 3.4: Average percent deviations of each group of perfluorocarbon droplets compared to week 0 at 4°C.....	44
Figure 3.5: Average percent deviations of each group of perfluorocarbon droplets compared to week 0 at 23°C.....	44
Figure 3.6: Average percent deviations of each group of perfluorocarbons compared to week 0 at 40°C.....	45
Figure 3.7: Size distributions by intensity of perfluorohexane sample stored in 4°C for 16 weeks.....	46
Figure 3.8: Size distributions by intensity of perfluorohexane sample stored in 23°C for 16 weeks.....	46

LIST OF FIGURES - Continued

Figure 3.9: Size distributions by intensity of perfluorohexane sample stored in 40°C for 12 weeks.....	46
Figure 3.10: Mechanical Index versus initial droplet diameter.....	47
Figure 3.11: Before and after pictures of an isolated and stable PFB droplet	49
Figure 3.12: Relationship between initial and final diameters in solution for PFCs with boiling points less than 37°C	49
Figure 3.13: Relationship between initial and final diameters in solution for PFMP droplets.....	50
Figure 3.14: Screenshot of computer software interface containing a) SEM image and b) EDS result obtained for PFB droplet sample	52
Figure 3.15: SEM and EDS results of PFB sample.....	52
Figure 3.16: TEM image of PFB droplet sample prepared at room temperature.....	53
Figure 3.17: Freeze-fracture TEM image of putative PFB droplets.....	54

LIST OF TABLES

Table 1.1: Imaging modalities and spatial resolution.....	14
Table 1.2: Chemical structures of perfluorocarbons used in this study.....	25
Table 1.3: Physical properties of perfluorocarbons.....	25

ABSTRACT

Microbubbles and nanodroplets are tools used in medicine for diagnosis and therapy. Probubbles are initially submicrometer droplets that become microbubbles in tumors as a result of ultrasonic force. The aim of this investigation was to determine vaporization thresholds of perfluorocarbon (PFC) droplets as a function of PFC boiling point and droplet size. PFC droplets with boiling points -1.7 to 56.6°C were formulated followed by acoustic droplet vaporization (ADV) and stability testing. Under ultrasound acoustic outputs used, perfluorohexane (PFH) droplets did not vaporize while perfluoro(-2-methyl-3-pentanone) (PFMP), perfluoropentane (PFP), and perfluorobutane (PFB) droplets did vaporize. The acoustic output required to vaporize droplets decreased with decreasing boiling point. Vaporization threshold is a function of size with larger diameter droplets requiring less ultrasound output to vaporize. PFH, PFMP, and PFP droplets remained stable after 16 weeks in 4°C and 23°C environments, but PFMP and PFP evaporated entirely in a 40°C oven after 12 weeks.

1. INTRODUCTION AND LITERATURE REVIEW: DESIGN RATIONALE

According to the latest SEER (Surveillance Epidemiology and End Results) report from the National Cancer Institute, it is estimated that 1.5 million people were diagnosed as having cancer in 2010 in the United States (Alekruse, *et al.*, 2009). Cancer is the uncontrolled growth of cells in terms of size and duplication where apoptosis (programmed cell death) is no longer in existence for such cells. As a result of uncontrolled growth, cancer cells oftentimes have the ability to spread to other areas of the body affecting other normal tissues in a process referred to as metastasis. Uncontrolled cell growth can also result in large masses of abnormal tissue known as tumors or neoplasms (Sticker and Kumar 2003). There are essentially two types of tumors, benign and malignant, for which four primary features can generally distinguish them: 1) differentiation and anaplasia: 2) rate of growth: 3) local invasion: and, 4) metastasis (Sticker and Kumar 2003). Tumors tend to promote angiogenesis resulting in being surrounded by “leaky vasculature” where the endothelial gap junctions are not as tight compared to areas where no tumor is present. Thus, the vasculature around a tumor is rather disorganized, distributed unevenly, and dependent on cell survival factors such as vascular endothelial growth factor (VEGF) in order to remain viable (Jain and Duda 2008). Such characteristics can be used as key markers in order to help detect and treat cancer.

Early detection and removal has been proposed as one of the methods to get rid of cancer especially prior to metastasis. There are biomarkers that can be identified in order to help identify cancer, a biomarker being any biological indicator that can be associated

with characteristics of tissue function. Some examples of biomarkers for some pathologies include changes in blood flow, blood perfusion, electrical activity, temperature, and pressure. In addition, there are many biomarkers for detecting early stage cancers, but few possess sufficient specificity and sensitivity needed for early stage detection. Even so, some methods of detecting cancer include detecting various biomarkers through blood chemistries, biopsies, and/or through the use of various imaging modalities such as computed tomography (CT), single photon emission computed tomography (SPECT), positron emission tomography (PET), optical imaging, magnetic resonance imaging (MRI), and ultrasound. An example of a biochemical biomarker includes prostate specific antigen (PSA) that can be detected via blood tests (Sticker and Kumar 2003). Biopsies (tissue samples) of cancer fixed onto microscope slides with stains such as hematoxylin and eosin are still a standard methodology for detecting abnormal cellular features mentioned earlier. Lastly, although imaging modalities alone could potentially detect some cancers, their effectiveness in terms of quality may be hindered by the non-specificity and lack of sufficient sensitivity of their imaging capabilities. Clearly, imaging can definitely be improved.

In order to enhance cancer cell imaging, contrast agents are usually necessary. For example, ultrasound imaging provides suboptimal images for echocardiography. Oftentimes, B-mode ultrasound offers equivocal information with regards to ventricular border definition and ventricular chamber delineation, and it offers no information regarding myocardial blood flow. Similar limitations can be seen for imaging the liver, kidney, and tissue. Today, microbubbles are common chemical contrast agents used to

enhance the suboptimal images by changing the acoustic impedance, which provides higher contrast and delineation of heart tissue (Section 1.1 has more details about this phenomenon). Furthermore, microbubbles can be used in conjunction with newer ultrasound pulse sequences to provide valuable information about myocardial and tissue blood supply as well as increased highlighting of tumor tissue.

Each imaging modality has advantages and disadvantages. In general, CT, SPECT, PET, optical imaging, and MRI scans can provide images of almost anything including bone and gas. However, CT, SPECT, PET, and MRI scans require patients to remain still making them less convenient. In addition, CT and SPECT machines are relatively expensive and require ionizing radiation that could potentially be mutagenic (Prince and Links 2006). Nonetheless, one of the most cost effective, safest, popular, and portable imaging modalities is ultrasound, which is not as invasive and is essentially risk free if used with clinically acceptable acoustic outputs (Prince and Links 2006). Ultrasound imaging is especially good for evaluation of pain and swelling, examining internal organs, and guiding biopsies because it exploits the advantages of non-invasiveness, convenience, and real-time imaging while avoiding or minimizing disadvantages of ionizing radiation, needles, and cost. Table 1.1 below displays the imaging modalities discussed and their corresponding sensitivities of usable concentrations of contrast agents per imaging modality.

Table 1.1. Imaging modalities and spatial resolution (¹Massoud and Gambhir 2003, ²Thomsen 2009, ³Blodgett 2010, ⁴Unger, *et al.*, 2003).

Imaging Modality	Contrast Agent	Dose Sensitivity (M) ¹	Duration ¹	Clinical Spatial Resolution (mm) ¹
CT	Iodine ²	10 ⁻³	minutes	0.05-0.2
SPECT	Iodine ¹	10 ⁻¹⁰ -10 ⁻¹¹	minutes	1-2
PET	¹⁸ F FDG ³	10 ⁻¹¹ -10 ⁻¹²	10 sec to minutes	1-2
MRI	Gadolinium-based ²	10 ⁻³ -10 ⁻⁵	minutes to hours	0.025-0.1
Ultrasound (5 MHz)	Perfluorocarbon microbubble ⁴	10 ⁻⁴ -10 ⁻⁵	seconds to minutes	0.05-0.5

Ultrasound uses a transducer to induce pressure sound waves, which are subsequently detected after reflecting off of objects (individual tissues interact in differential ways with sound) in order to create an image of a localized region of tissue. A piezoelectric transducer induces set frequencies (MHz) and power (W/cm²), which creates the pressure waves in addition to receiving reflective sound energy from the areas of interest (Prince and Links 2006). The US Food and Drug Administration (FDA) has indicated the Mechanical Index (MI) (Equation 1) as an important ultrasound parameter because of the desire to prevent potential bioeffects (Section 1.5). Typical mechanical indices in clinical settings range from 0.05 to an FDA approved maximum of 1.9.

$$MI = \frac{p_r}{\sqrt{f}} \quad \text{Equation 1}$$

where p_r : peak negative pressure (MPa)
 f : center frequency (MHz)

1.1. Vascular Contrast Agents

In general, vascular contrast agents are injected intravenously (i.v.) into the vascular space in order to help provide better contrast when imaging the cardiovascular

system. Vascular contrast agents can be used for numerous applications including direct diagnoses and treatments. Various imaging modalities have their own corresponding contrast agents. Each contrast agent alters the energy (absorption, relaxation, reflection, or emission) provided by the imaging modality, which thereby provides contrast in order to assist physicians in visualizing a region of interest (ROI). For example, the vascular contrast agents for CT have generally been iodine-based where the x-ray beams become weakened and contrast increases. The vascular contrast agents for MRI have been gadolinium-based, which shorten the relaxation times of hydrogen nuclei of water molecules. Most of the vascular contrast agents for ultrasound are microbubbles although there has been some interest in echogenic liposomes (ELIPS) as well (Alkan-Onyuksel, *et al.*, 1996).

Microbubbles are primarily lipid-coated bubbles that are used as ultrasound contrast agents and are filled with air, perfluorocarbon gas, or sulfur hexafluoride. Furthermore, the gas solubility properties of the gases in the aqueous milieu are one component that determines their circulating lifetime. Other factors include microbubble size (smaller size results in less susceptibility to elimination via the reticuloendothelial system [RES]) and lipid composition (microbubble membranes with polyethylene glycol [PEG] offer “stealth” qualities so as to not be recognized by the RES). The gases used in microbubbles work by increasing the backscattered echoes at the gas-water interface (impedance mismatch) during ultrasonic imaging. The first reported use of a microbubble was in 1968 when Gramiak and Shah injected air bubbles produced by quick injection of saline into the aortic root (Gramiak and Shah 1968). From there, the

field of ultrasound contrast agents gained interest, and now, there are several ultrasound contrast agents on the market for clinical use. Most of the ultrasound contrast agents are microbubbles that are injected i.v. and assist in ultrasonography by exhibiting a different reflection of sound energy (change in acoustic impedance at the gas-liquid interface) while providing high contrast and delineation of diseased tissues within the cardiovascular system.

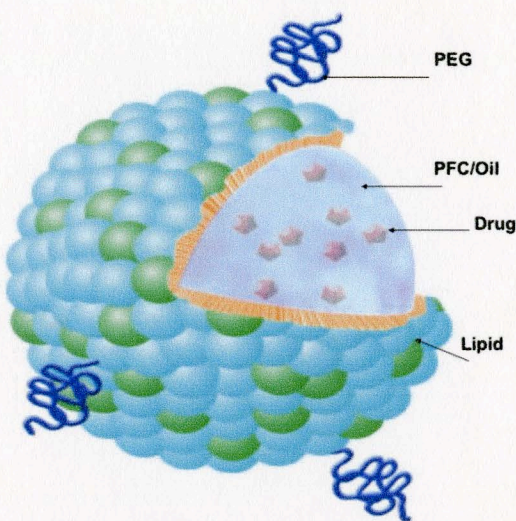


Figure 1.1. Microbubble with lipid shell and gaseous perfluorocarbon (PFC) core. Polyethylene glycol (PEG) tail is used for stealth and potential ligand attachment for cell specificity, and oil is used to help internalize and stabilize a potential drug.

According to Albers in 1960, the backscatter of a bubble in the Rayleigh scattering regime is related to the sixth power of the bubble radius, which suggests that large decreases in backscatter can occur with slight decreases in bubble radius (as cited in Wei, *et al.*, 1998). Specifically, the contrast is due to an occurrence known as Rayleigh scattering. Rayleigh scattering occurs especially with microbubbles because of their extreme difference in acoustic impedance compared to blood and tissue. This impedance also causes a difference in backscattering of ultrasound that results in visibility even at

low mechanical indices. If the particles (microbubbles) are much larger causing backscattering of ultrasound at higher angles, then the type of scattering is referred to as Mie scattering. Both are the theories involved that help explain the mechanism behind the contrast shown in ultrasound images provided by microbubbles.

Despite their utility as vascular contrast agents, one of the limiting factors of microbubbles is their diameter ($\sim 1\text{-}5\ \mu\text{m}$), which limits their use to the intravascular space. As mentioned earlier, larger microbubbles provide more contrast via ultrasound imaging, but the size must be limited to a maximum diameter to allow unobstructed flow through the capillaries. Alternatively, even $1\ \mu\text{m}$ diameter bubbles may be too large for extravasation outside “leaky” vasculature according to one study, which has founded that $780\ \text{nm}$ diameter particles may be the largest to passively diffuse into the tumor site (Hobbs, *et al.*, 1998). However, there is no specified size threshold that can be defined with passive diffusion through “leaky” vasculature because it is dependent on numerous factors including the stage of the tumor, the number of microbubbles involved, and how much time is necessary to allow for microbubbles to accumulate within or near the tumor site. Therefore, it is important to identify that it is currently unknown as to what ideal size would be necessary in order to passively diffuse to the extravascular space for any tumor. Also, although one $1\ \mu\text{m}$ diameter microbubble is sufficient to be detected on the ultrasound image, a plethora of microbubbles cannot passively extravasate to the extravascular space and an alternative design approach may be needed.

1.2. Perfluorocarbons

Typically, perfluorocarbons (PFCs) have been used as the primary gas for vascular

contrast agents because they are essentially inert and will not be converted with any human metabolic function (Spahn, *et al.*, 1994 and Keipert 1998). Not being metabolized presents an advantage when used as an imaging tool as it will eventually become excreted unchanged through the lungs over time. Even though perfluorocarbons are amphiphobic (dislike nearly everything), their stability in microbubbles is due to: 1) their virtual insolubility in water, and 2) their encapsulation in a shell. Furthermore, their elastic properties also enhance their echogenicity, which in turn provides better contrast during ultrasonic imaging. Nonetheless, they still need to be encapsulated by either polymeric shells or surfactants to reduce the interfacial tension between water and perfluorocarbons. The reduction in surface tension results in a reduction in Laplace pressure, which assists in stabilizing bubbles, especially the smaller ones. Laplace pressure is the difference between the pressure inside of a droplet/bubble and the pressure outside of a droplet/bubble. A surfactant such as a lipid coating would not only be necessary to encapsulate perfluorocarbons but also to stabilize lower boiling perfluorocarbons in order to prevent from them vaporizing too soon.

The membrane coating of encapsulated perfluorocarbons could vary depending on the contents and phases of the internal core and surrounding environments. Most perfluorocarbon bubbles tend to be comprised of a lipid monolayer membrane, so they could conceivably be referred to as gas-filled micelles (Singhal, *et al.*, 1993). Liposomes typically have lipid bilayers similar to cellular structures with polar heads facing inwards and outwards because the aqueous milieu is both internal and external. The perfluorocarbon emulsions (droplets) tend to involve a monolayer even though

perfluorocarbons are amphiphobic.

1.3. Requirements for Vascular Diffusion

In order to extravasate out of the vasculature and passively diffuse to an area of disease or tumor, microbubbles must either have small diameters (hundreds of nm) or begin as a smaller particle such as a droplet (also hundreds of nm). Typically, the vasculature near an area of disease or tumor is “leaky” such that the spacing of the endothelial gaps is larger than normal. Another term for this characteristic is increased vascular permeability. Some studies suggest that the lengths of the intercellular endothelial gaps of “leaky” vasculature can be as small as 30 nm and as large as 780 nm (Mayer, *et al.*, 2002; Hobbs, *et al.*, 1998) although these still have not been defined and are dependent on the stage of the tumor. Thus, the vasculature for tumors remains permeable due to several factors such as vascular endothelial growth factor (VEGF), bradykinin (BK), and nitric oxide (NO) to maintain pathways for nutrients for the tumor cells (Maeda, *et al.*, 1994). Along with the permeability factors, it appears that macromolecules and lipids accumulate in tumor tissue and remain for long time periods (Matsumura and Maeda, 1986). This characteristic is commonly referred to as the enhanced permeability and retention (EPR) effect (Matsumura and Maeda, 1986). It is the EPR effect near tumor sites that many scientists would like to exploit, especially with regards to cancer therapeutics. Therefore, several devices have been developed in an effort to help diagnose and treat cancer including microbubbles and emulsion droplets.

1.4. Requirements for Ultrasound-Mediated Vaporization

In general, droplets are defined as bodies of liquid suspended within another liquid.

Frequently, droplets are created via emulsion chemistry with two immiscible liquids such as either oil-in-water or water-in-oil, and they form because of the interfacial tension that exists between the two liquids (McClements, 2005). In this case, droplets are typically smaller than microbubbles having diameters $< 1 \mu\text{m}$ and they contain a perfluorocarbon liquid core rather than a gaseous core. However, it is possible to make droplets to have diameters in the micrometer range as well. As microbubbles are typically restricted to the vasculature due to their size, droplets that have hundred nanometer diameters are capable of passively diffusing through the intercellular endothelial gap junctions and into the extravascular space (Dayton, *et al.*, 2006). Because of their ability to move beyond the extravascular space, their potential application as therapeutic drug deliverers and imaging agents is further expanded.

1.5. Potential Bioeffects

No imaging modality, including ultrasound, is one hundred percent safe, and there are potential bioeffects. Bioeffects can occur as a result of an imaging device affecting normal cells and tissues that cause abnormalities over time. The goal of my project was to design a droplet that can undergo non-inertial cavitation into a microbubble using a low MI as this lowers the probability of having bioeffects. Ultrasound alone provides both thermal and mechanical energy that can be transferred to cells. The amount of energy can increase the temperature in cells that can eventually be damaging. The thermal index (TI) represents the amount of heat energy applied to tissues (Equation 2) and has been used concurrently with the MI to monitor applications of ultrasound energy. Although the MI remains as the primary indicator currently used on most ultrasound

machines, the MI might not be the best indicator of ultrasound energy because there appears to be no direct relationship between MI and microbubble cavitation (Forsberg, *et al.*, 2005).

$$TI = \frac{W}{W_{\text{deg}}} \quad \text{Equation 2}$$

where W: total acoustic power

W_{deg} : acoustic power required

to raise the temperature of tissue 1°C

Some bioeffects may include a number of abnormal biological alterations to molecular and/or cellular structures. Heating causes bioeffects by increasing the temperature higher than the normal physiological temperature. Reports of consequences from heating mainly involve embryonic development in animals (Barnet, *et al.*, 1997, Barnett, *et al.*, 2000, and Ziskin 1999). In addition, heating can promote inflammation (Speed 2001), wound repair (Speed 2001 and Jackson, *et al.*, 1991), and production of heat shock proteins (Barnett, *et al.*, 1990 and Walsh, *et al.*, 1987). Most reports of bioeffects from cavitation refer to inertial cavitation of microbubbles where the microbubbles are disrupted. The bioeffects from cavitation are stimulations of arteriogenesis and angiogenesis (Song, *et al.*, 2002, Song, *et al.*, 2004, and Skyba, *et al.*, 1998). More importantly, cavitation of microbubbles after application of ultrasound can rupture the surrounding endothelial membrane (Skyba, *et al.*, 1998). Therefore, it is important that the probubble design can undergo non-inertial (stable) cavitation and inertial cavitation under conditions that will be as minimally damaging as possible.

1.6. Design Proposal

We propose that a probubble can be designed to act as a potential diagnostic and/or therapeutic tool. The probubble is initially a droplet that contains a lipid shell with a liquid perfluorocarbon core and is small enough to passively diffuse into the extravascular space, especially near a tumor site. A polyethylene glycol tail can be attached to the lipid pointing outwards for stealth and to allow for potential attachment of a ligand that would be specific to the particular target cancer cell. The droplet will then attach to the receptor of the target cell. Furthermore, uptake enhancers such as folic acid may also be incorporated onto the droplet surface to enhance internalization. Once the droplet has been internalized into the target cell (after 1-2 days to allow for circulation, EPR effect, and physiological washout), an ultrasonic pulse will provide thermal and mechanical energy specific for the droplet in order to induce non-inertial cavitation of the droplet into a microbubble, which will cause the liquid core to become a gas core resulting in expansion of the droplet into a microbubble. Thus, the microbubble will not be disrupted and remain stable for the duration of ultrasound imaging.

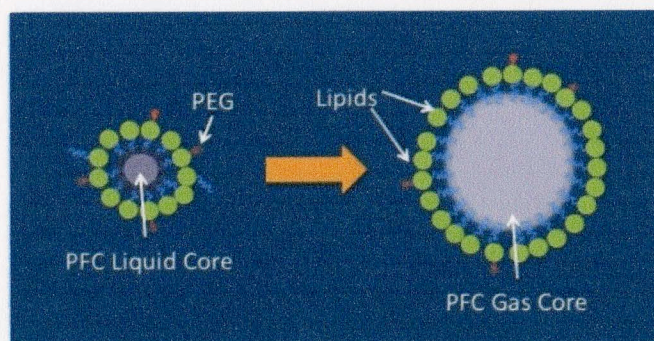


Figure 1.2. Probubble design in initial and final states. Initial state is on left indicative of perfluorocarbon-filled droplet due to liquid core and smaller diameter. Final state is on right indicative of perfluorocarbon microbubble due to gaseous core and larger diameter (approximately 5 times greater than droplet diameter). Probubble contains lipid shell for added stability with polyethylene glycol (PEG) tails for potential ligand attachment. Conversion from droplet to microbubble will occur after application of ultrasound energy.

Once the gas core results in at least a 1 μm in diameter microbubble, the ability to view the microbubble via ultrasonic imaging is feasible, revealing the location of the target cell if the ligand-receptor moiety is target-specific and not found in normal cells. This may help diagnose several different types of diseases much less invasively than other procedures such as biopsies, and this should also be a cheaper alternative than CT and MRI. As far as therapeutic applications, once the microbubble is visible in the ultrasound display, an increase in MI should allow further inertial cavitation of the microbubble (Holland and Apfel 1990) into a larger volume to occupy space of the target cell eventually destroying only the target cells as the microbubble collapses (Figure 1.3). However, numerous microbubbles must be internalized in one target cell for ablation because the cells are at least 10 μm in diameter. Alternatively, the microbubbles themselves can potentially serve as toxins to the tumors cells depriving them of nourishment and preventing further growth.

However, it is necessary to learn more about these droplets and determine if they are able to perform each sequence in the probubble application. Here, we want to address the following: 1) vaporization as a function of average diameter, 2) vaporization as a function of boiling point, and 3) stability of droplets. Although some generalizations can be made about the membranes of the droplets being monolayer, bilayer or multilayer, the formulation here is somewhat different from other droplets. Therefore, some assumptions will be made about these droplets. For example, the droplets are essentially emulsions and will be assumed to take on spherical structures. In addition, it will be assumed that the droplets can be reproduced with uniform size (see Section 2.1).

Primarily, it is important to identify the vaporization thresholds of these droplets as a function of size and boiling point. Secondly, the storage stability of these droplets will be investigated. The stability will be determined by how well these droplets maintain their sizes over time in a specified temperature environment. These experiments involve four different perfluorocarbons (Table 1.2), which have different structures and boiling points (Table 1.3) that may affect their stability.

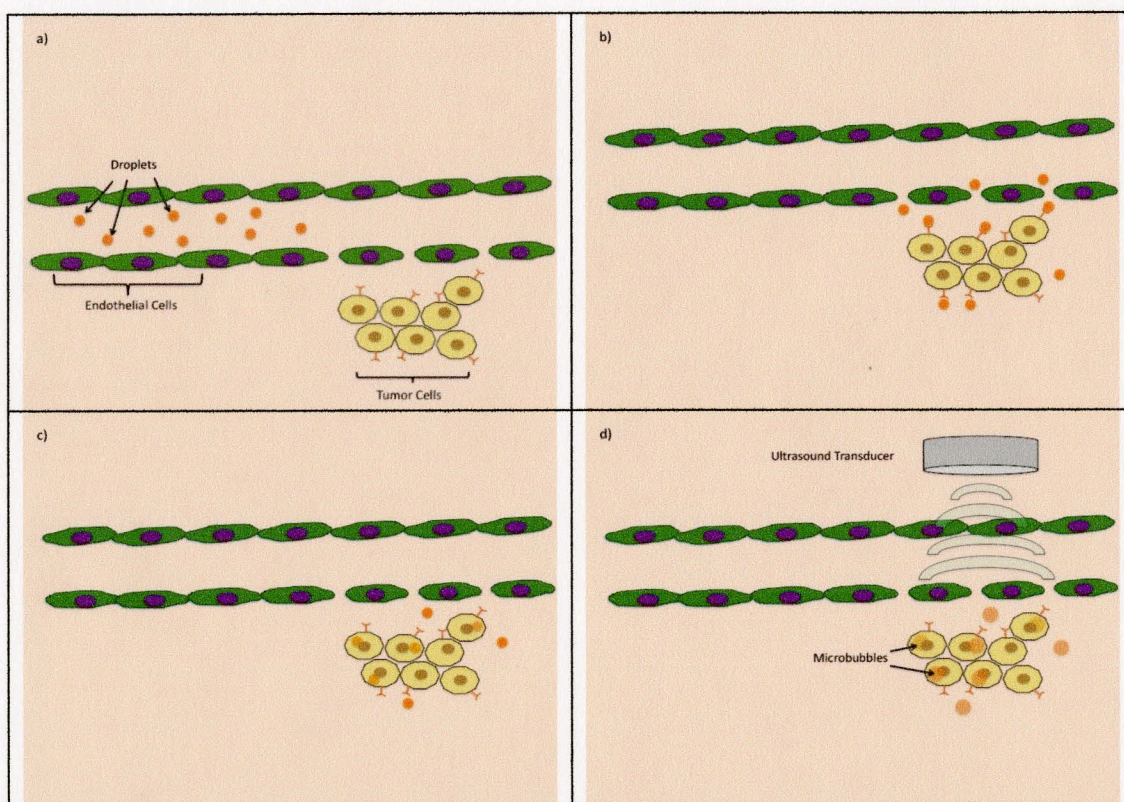


Figure 1.3. Schematic of *in vivo* application of probubble precursor design. (a) Droplets traveling intravenously. (b) Droplets passively diffusing to extravascular space and binding to tumor cell receptors. (c) Droplets are internalized into tumor cells. (d) After 1-2 days to allow time for circulation, EPR effect, and physiological washout, ultrasonic force is applied to provide thermal and mechanical energy for droplets to undergo non-inertial cavitation into microbubbles.

Table 1.2. Chemical structures of perfluorocarbons used in this study.

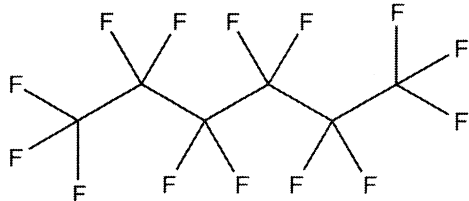
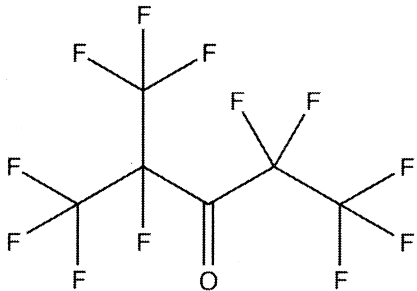
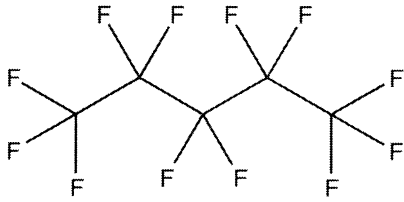
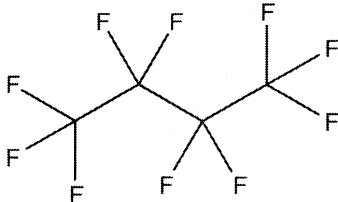
Perfluorocarbon	Chemical Structure
Perfluorohexane	
Perfluoro(2-methyl-3-pentanone)	
Perfluoropentane	
Perfluorobutane	

Table 1.3. Physical properties of perfluorocarbons (⁵Lide 2010, ⁶Chemical Book 2008b).

Popular name (acronym)	CAS number	Molecular formula	Boiling point (°C)	Liquid Density (g/mL)	Molecular weight (g/mol)
Perfluorohexane ⁵ (PFH)	355-42-0	C ₆ F ₁₄	56.6	1.71	338
Perfluoro(2-methyl-3-pentanone) ⁶ (PFMP)	756-13-8	C ₅ F ₁₂ O	49.2	1.6	316
Perfluoropentane ⁵ (PFP)	678-262	C ₅ F ₁₂	29	1.63	288
Perfluorobutane ⁵ (PFB)	355-25-9	C ₄ F ₁₀	-1.7	1.594	238

1.7. Theory

1.7.1. Ideal Gas Law and Non-inertial Cavitation

It is assumed that perfluorocarbon gases obey the ideal gas law (Equation 3). Therefore, the volume expansion of a PFC droplet can be determined.

$$PV = nRT \quad \text{Equation 3}$$

P is the pressure in atmospheres, V is the volume in liters, n is the number of moles of perfluorocarbon, R is the gas constant, and T is the temperature in Kelvin. The following is an example forming a large bubble starting from a droplet that is 200 nm in diameter:

Starting with a 200 nm diameter droplet and neglecting the thickness of the membrane, the spherical volume is 4.2×10^{-15} mL.

If the perfluorocarbon is a liquid, the number of moles of perfluorocarbon could be calculated based on the liquid density and molecular weight of perfluorocarbon (properties listed in Table 1.3). Average normal body pressure is roughly 90 mm Hg (0.12 atm) and will be deemed negligible for these calculations.

$$n = 4.2 \times 10^{-15} \text{ mL} \times \frac{1.63 \text{ g PFP}}{\text{mL}} \times \frac{\text{mol PFP}}{288 \text{ g PFP}} = 2.4 \times 10^{-17} \text{ mol PFP}$$

Assume P = 1 atm and T = 310.13 K (37°C)

Use R = 0.0821 L•atm/mol•K and use Equation 3 to solve for V:

$$V = \frac{nRT}{P} = \frac{2.4 \times 10^{-17} \text{ mol PFP} \times 0.0821 \text{ L} \cdot \text{atm/mol} \cdot \text{K} \times 310.13 \text{ K}}{1 \text{ atm}}$$

$$V = 6.0 \times 10^{-16} \text{ L} = 6.0 \times 10^{-13} \text{ mL} = 6.0 \times 10^8 \text{ nm}^3$$

Solve for final diameter (d_f) using final volume

$$V = 6.0 \times 10^8 \text{ nm}^3 = \frac{4}{3} \pi r^3$$

$$r_f = \sqrt[3]{\frac{3V}{4\pi}} = \sqrt[3]{\frac{3 \times 6.0 \times 10^8 \text{ nm}^3}{4\pi}} = 524.3 \text{ nm}$$

$$d_f = 2r_f = 2 \times 524.3 \text{ nm} = 1048.6 \text{ nm}$$

Compare the initial and final diameters to determine the expansion factor:

$$\frac{d_f}{d_i} = \frac{1048.6 \text{ nm}}{200 \text{ nm}} = 5.243$$

Therefore, the increase in bubble size from droplet diameter should be around a factor of 5.2. When considering all of the perfluorocarbons, the range of increases is around 5-5.5 (Appendix A) times the original droplet diameter depending on initial droplet size or, more directly, the initial amount of perfluorocarbon. Thus, a 1 μm diameter bubble should derive from approximately a 200 nm diameter droplet.

1.7.2. Perfluorocarbon Droplet Diameter Based on Vapor Pressure

The vapor temperature of perfluorocarbons can be estimated as a result of encapsulation within a membrane (Rapoport, *et al.*, 2009). This relationship is a modified version of the Antoine equation (Equation 4) where Laplace pressure is taken into consideration.

$$\log_{10} P = A - \frac{B}{T + C} \quad \text{Equation 4}$$

where P: vapor pressure

T: absolute temperature (K)

A,B,C: Antoine equation constants particular for a substance

It is assumed that the membrane is a solid structure to approximately account for Laplace pressure. Therefore, the vapor pressure can include Laplace pressure, which is a difference in pressure (Equation 5).

$$\Delta P = P_{inside} - P_{outside} = \frac{2\sigma}{r} \quad \text{Equation 5}$$

where P_{inside} : pressure inside the droplet
 $P_{outside}$: pressure outside of the droplet
 σ : surface tension
 r : droplet radius

Incorporating in Equation 5 into Equation 4, where ΔP will be included in P (now the absolute pressure, which is the sum of atmospheric, body, and droplet pressures) provides a relationship of vapor temperature as a function of droplet radius (Equation 6).

$$T = \frac{B}{A - \log_{10}\left(P_{atm} + P_{body} + \frac{2\sigma}{r}\right)} - C \quad \text{Equation 6}$$

So, the vaporization temperature (T) of a droplet can be estimated from the droplet's size. The surface tension for the lipids used in this study is typically 51 mN/m, and the component constants were taken from NIST Chemistry Webbook (Linstrom and Mallard 2010). Figure 1.4 shows the relationship between the vaporization temperature and the droplet diameter based on the Antoine equation relationship (Equation 6) for various perfluorocarbons. Theoretically, perfluoropropane has the potential to become encapsulated within a droplet that is 100 nm in diameter, which is estimated to have a vapor temperature of 35°C. Thus, the other PFC droplets could potentially be

encapsulated at room temperature while their vapor temperatures are much higher than perfluoropropane for 100 nm droplets.

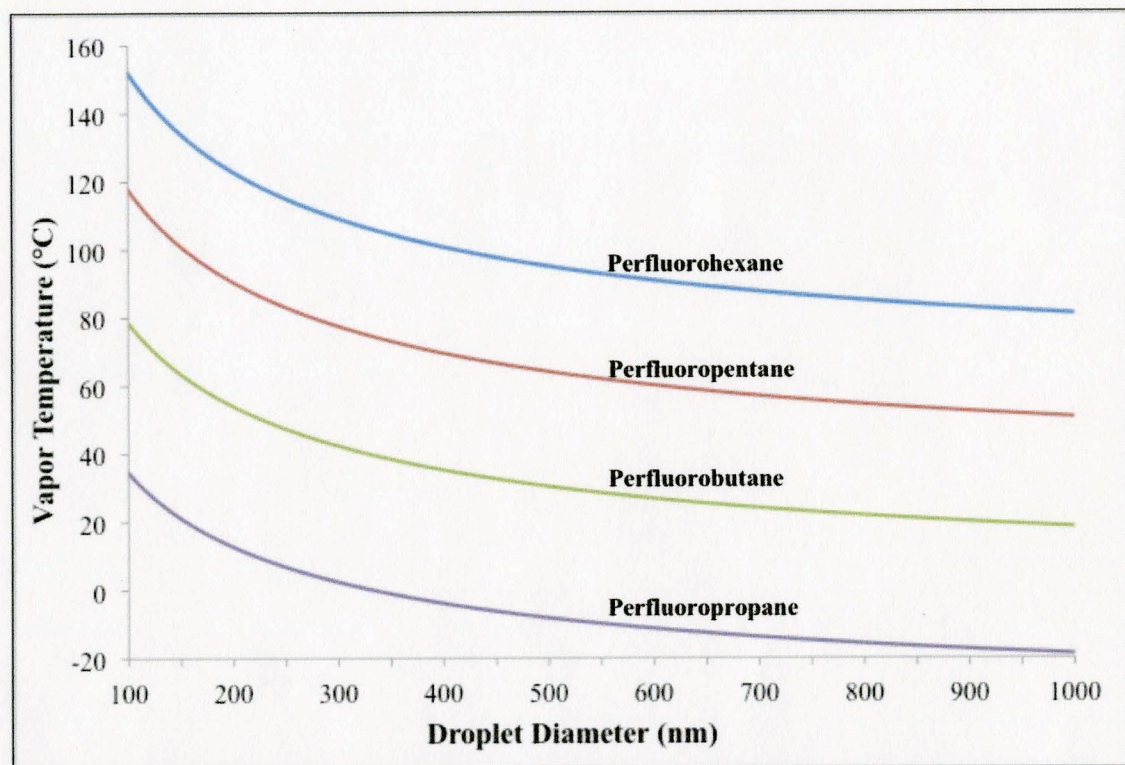


Figure 1.4. Estimated vapor temperature of perfluorocarbon within a droplet. The corresponding Excel setup can be found in Appendix B.

1.8. Prior Works

There have been several studies of droplets and their conversions to microbubbles performed in the past decade. For example, some studies have involved the targeting of drugs directly to the tumor site via nanoparticle precursors (Nam, *et al.*, 2009). The main differences between their design and the one proposed here are the membrane structures and how the droplets are prepared. Other studies use biodegradable block copolymers that resemble lipid structures (Gao, *et al.*, 2008, Nam, *et al.*, 2009), and they rely on the self-assembly of droplets due to the natural interactions between the perfluorocarbons,

block copolymers, and aqueous solution without a controlled homogenization technique, such as the use of a membrane for predetermined sizes. Thus far, the studies have found that their droplets can convert to nano/microbubbles upon heating, and the nanobubbles do coalesce to form larger, visible bubbles (Gao, *et al.*, 2008). They were even able to design a tumor-selective droplet (Gao, *et al.*, 2008). Sonication was the most efficient for non-inertial cavitation of a droplet to a microbubble (Rapoport, *et al.*, 2009), which supports the reasoning for our device design.

Kripfgans and coworkers have studied larger droplet sizes ($> 4 \mu\text{m}$) that would be limited to the vascular space design especially for occlusion therapy in capillary beds (Kripfgans, *et al.*, 2000, Kripfgans, *et al.*, 2002). Their droplets were developed with perfluoropentane and a shell of denatured albumin. These researchers found that an increase in acoustic intensity was required for expanding smaller droplets (Kripfgans, *et al.*, 2004), which supports our design rationale.

1.9. Specific Aims and Hypotheses

Specific Aim 1: To determine the stability of droplets with similar lipid composition but different perfluorocarbon core content, and to determine the stabilities of perfluorocarbon droplets under different temperatures over a period of 16 weeks. A similar study was done where the stability of 1,2-trans(bisperfluorobutyl)ethylene droplets was monitored (Burgess and Yoon 1995). Our studies expand their report by using various perfluorocarbons and methods to obtain more uniform samples.

Hypothesis: We hypothesize that the perfluorohexane droplet will show the greatest stability relative to the other perfluorocarbon droplets due to its higher boiling

point. The other perfluorocarbon droplets will expand due to being more volatile (lower boiling points) compared to perfluorohexane.

The stability of the droplets will be monitored via the Malvern Zetasizer Nano ZS particle size machine. It provides an inherent standard error of ± 10 percent from the standards of 100 nm, 200 nm, and 400 nm reference beads (NanosphereTM Size Standards – 3000 Series, Thermo Scientific, Fremont, CA). A sample of droplets will be determined to be stable if the droplets maintain the same z-average size (average diameter based on dynamic light scattering intensity) or size profile (size distribution of sample based on intensity) over time compared to its z-average baseline value within a 10 percent standard error.

Specific Aim 2: To determine the vaporization threshold of droplets as a function of diameter, boiling point, and partial pressure.

Hypothesis: The vaporization threshold of droplets with perfluorocarbons of higher boiling points will be much higher than those droplets with perfluorocarbons of lower boiling points as predicted by the Antoine equation. Ultrasound energy induces mechanical and thermal effects that can cause liquid perfluorocarbons to vaporize. Perfluorohexane has the highest boiling point of the group of perfluorocarbons to be tested and, thus, should be more difficult to vaporize than a perfluorocarbon having a lesser boiling point. Droplets that require mechanical indices less than 1.9 will be considered for eventual *in vivo* studies.

Specific Aim 3: To encapsulate liquid perfluorobutane within lipid shells in order to form metastable droplets.

Hypothesis: We hypothesize that we can make metastable droplets that match our criteria of stability and vaporization. A perfluorocarbon with a boiling point less than room temperature may be stabilized in lipid shells or emulsions as a metastable droplet for use at body temperature (37°C). Such a droplet would be potentially beneficial by allowing use of less ultrasonic output energy in order to limit or eliminate bioeffects.

2. MATERIALS AND METHODS

2.1. Preparation of Perfluorocarbon Droplets

Initially, lipid thin films were prepared with a composition containing 85 mole percent dipalmitoylphosphatidylcholine (DPPC), 10 mole percent 1-palmitoyl-2-hydroxy-*sn*-glycero-3-phosphocholine (LPC), and 5 mole percent 1,2-dipalmitoyl-*sn*-glycero-3-phosphoethanolamine-N-[methoxy(polyethylene glycol)-2000] (DPPE-PEG 2000) (Avanti Polar Lipids). The lipids were dissolved in less than 1 mL of chloroform (EMD Chemicals) and gently evaporated with nitrogen gas. The lipids were lyophilized (VirTis Freezemobile 25EL Sentry 2.0 Lyophilizer) overnight to remove residual solvent and create lipid films.

The lipid films were rehydrated with approximately 1 mL of HEPES (4-(2-hydroxyethyl)piperazine-1-ethanesulfonic acid) buffer (pH = 7.4) and sonicated for 10 minutes in a water bath sonicator (Branson 1510, Danbury, CT) at 50-60°C. The rehydrated films were subjected to 10 freeze-thaw cycles, first freezing with an isopropanol bath with dry ice followed by thawing with a 50-60°C water bath. This created a homogeneous lipid suspension, which was also stirred for 10 minutes at 50-60°C immediately afterwards. The resulting concentration of the lipid solution was about 20 mg/mL.

The perfluorocarbons used were perfluorohexane (PFH), perfluoro(2-methyl-3-pentanone) (PFMP), and perfluoropentane (PFP). PFH and PFP were purchased from FluoroMed (Round Rock, TX). PFMP was purchased from SynQuest (Alachua, FL). Their physical properties are listed in Table 1.3. Each perfluorocarbon was added to the

lipid solution (20% v/v), and multiple extrusions were performed using an Avanti Mini-Extruder (Avanti Polar Lipids, Alabaster, AL) with polycarbonate membrane filters (Whatman Nuclepore Polycarbonate Track-Etch Membrane) at room temperature (23°C). Membrane filters with 200 nm pores were used for stability tests, and filters with 1 μm pores were used for acoustic droplet vaporization (ADV). Normally, extrusions would occur at temperatures above the phase transition temperature of the lipids, but we performed the extrusions at room temperature due to the boiling point of PFP. Extrusions were completed after 20 passes through the membrane. The resulting solutions underwent centrifugation (Beckman Model TJ-6 Centrifuge) for 15 minutes and between 800 and 1000 rpm. For stability tests, the samples were stored immediately in a refrigerator at 4°C, in a styrofoam container at 23°C, or in an oven at 40°C. For ADV tests and further sizing, the samples were stored in a styrofoam container with a refrigerated ice pack and sent to Dr. Paul Dayton's laboratory located at the University of North Carolina (UNC).

2.2. Preparation of Perfluorobutane (PFB) Droplets

For the PFB droplets, the same lipid solutions were used, but the procedures differed when introducing the PFB. First, the PFB gas (FluoroMed, Round Rock, TX) was condensed in an Exacta-MixTM EVA Container over dry ice. The condensed PFB was poured into a 2 mL glass vial and crimped. It was impossible to perform an extrusion after adding the PFB to the lipid solution. Instead, the lipid solution was added to condensed PFB in the glass vial and shaken on a modified "dental shaker" (VialmixTM,

120V/60Hz, Bristol-Myers Squibb Medical Imaging, Inc., North Billerica, MA) for 45 seconds.

As a modification to the above methodology, glycerol (Sigma) was added to the lipid solution (20% by volume) prior to performing the extrusion. Glycerol is commonly used as a cryoprotectant for blastocysts (Cohen, *et al.*, 1985 and Fehilly, *et al.*, 1985). Thus, it should most likely provide a protective shell around the lipid membrane in addition to the liquid PFB. Similarly, methods presented by Pan and Wang (Wang and Pan 1994 and Pan, *et al.*, 1999) introduced their use of glycerol to make superheated-liquid droplets of Freon-12, which has a boiling point of -29.8°C (Lide 2010).

Upon entering a -20°C walk-in freezer, 200 μL of PFB was extracted and added to the lipid solution. A 13 mm diameter syringe holder (KS13, Advantec MFS, Dublin, CA) was used instead of the Avanti Mini-Extruder where an additional female luer-lok was attached to the outlet with the appropriate male luer slip. Here, a 1 μm porous membrane filter was also used, and extrusions were completed after 20 passes through the membrane. The emulsion was placed in a 2 mL vial, crimped, and stored at 4°C . Storing the resulting emulsion at -20°C would cause the lipids to potentially fall out of position as they thaw.

2.3. Identification of Droplet Storage Stability

The Malvern Nano ZS particle size analyzer (Malvern Instruments Ltd., Malvern, Worcestershire, UK) has an inherent standard error of 10 percent with standards of 100 nm, 200 nm, and 400 nm reference beads (NanosphereTM Size Standards – 3000 Series, Thermo Scientific, Fremont, CA). The stabilities of the perfluorocarbon droplets were

determined based on how long the droplets maintained their z-average sizes over time within 10 percent from their baseline z-average sizes. Z-average size is a mean diameter based on the intensity of the dynamic light scattering result from a given sample. Perfluorocarbon emulsions were prepared specifically for sizing via dynamic light scattering on the particle size analyzer. Briefly, 150 microliters of sample was introduced into a 12 mm disposable square polystyrene cuvette, 1 mL of HEPES buffer was added, and the cuvette was capped. The z-average sizes were monitored immediately after preparation (week 0), week 2, week 4, week 8, week 12, and week 16. Sixteen weeks would represent a short-term storage stability study following FDA guidelines for drug stability (Bensley 2008). Raw data and data analysis for the stability study can be found in Appendix C.

2.4. Scanning Electron Microscopy (SEM)

SEM was performed at the University Spectroscopy and Imaging Facilities (USIF) at the University of Arizona. A drop of each sample (PFP or PFB droplets) was spread over a 1 cm² piece of silicon on top of an aluminum stub. The samples were then left to dry under a fume hood where the PFP sample remained as a thin layer of liquid solution whereas the PFB sample became foamy in appearance as a result of the drying process. The samples were coated with platinum under a plasma chamber for about 10 minutes. Samples were examined under SEM (Hitachi S-4800 Type II) simultaneously along with the energy dispersive x-ray (EDS) analyzer (ThermoNORAN NSS EDS), which was used to further confirm SEM results. Primarily, detection of fluorine was used

as a key indicator for the presence of any perfluorocarbon. All samples were viewed with back-scattering electrons.

2.5. *Transmission Electron Microscopy (TEM)*

Oftentimes, it is necessary to perform freeze-fracture transmission electron microscopy (TEM) in order to maintain the inherent integrity of cellular structures or, in this case, emulsions. However, Chetanachan *et al.* (2008) suggested a potential negative staining technique to visualize liposomes via TEM at room temperature. Even though droplets are essentially emulsions and are not bilayer structures like liposomes, both contain lipid membranes that can be stained for TEM. Therefore, a similar method was used with a few slight modifications to the procedure.

TEM was performed at USIF at the University of Arizona. Briefly, PFP and PFB droplets were prepared by inserting a drop of perfluorocarbon droplet solution between a 0.5 cm² carbon and mica layer (the sample diffused through the spacing between the substances). The carbon-sample-mica segment was inserted at a 45° angle into a small well of 2% phosphotungstic acid (pH = 7.4) for staining of the phospholipids. This also allowed for the carbon layer to float across the top of the well containing the sample. The carbon layer was scooped up with a 400 mesh copper grid and wicked onto filter paper. The sample was ready for TEM analysis using a JEOL 100CX II TEM.

2.6. *Freeze-Fracture TEM*

Dr. Brigitte Papahadjopoulos-Sternberg did the freeze-fracture TEM. PFB droplets were prepared for freeze-fracture TEM using a quenched sandwich technique employing liquid nitrogen-cooled propane at a cooling rate that avoids ice crystal

formation and artifacts secondary to the cryofixing process. Samples were processed within two hours after liquid nitrogen storage. Fracturing was conducted using a JEOL JED-9000 with freeze etching and fracture planes shadowed with platinum for 30 seconds at an angle of 25° to 35° followed by treatment with carbon for 35 seconds. Replicas were cleaned with fuming nitric acid and chloroform/methanol. Images were examined on a JEOL 100CX TEM.

2.7. Experimental Apparatus

Perfluorocarbon droplet samples were shipped to Paul Sheeran at the University of North Carolina (UNC) in a styrofoam container along with a refrigerated gel pack. All apparatus for acoustic droplet vaporization (ADV) tests were designed and constructed by Paul Sheeran in the laboratory of Professor Paul A. Dayton at UNC. According to Sheeran and colleagues, “a water bath constructed of acrylic was mounted on top of an inverted microscope (Olympus IX71) and interfaced with a high-speed camera (FastCam SA1.1, Photron USA, Inc.) to capture monochrome videos and still images of particles and microbubbles. A 100X NA=1.0 water immersion objective was used to provide image magnification. The optical resolution of the system was measured to be 0.5 μm , as determined by a calibrated line pair test slide (Max Levy Autograph, Inc.). Baseline water oxygen saturation was measured to be 5 PPM at 37°C, as measured by a chemical test kit (Oxygen CHEMets, CHEMetrics, Inc). In the case of degassed experiments, an in-line degasser was allowed to operate until the water oxygenation in the water tank measured less than or equal to 1.5 PPM. The water bath was passively heated to a consistent 37°C by heating water in an auxiliary tank and continuously pumping it

through copper coils lining the main tank such that vibration in the water bath was minimized (Figure 2.1). The temperature of the auxiliary tank was adjusted until the desired temperature of the water in the experiment region of the main tank along with any additional light heating was reached. The droplet solution was pumped through a nearly optically and acoustically transparent cellulose tube with a 200 μm inner diameter (Spectrum Labs, Inc.) using a custom-built manual injector allowing for precise administration of the droplets into the field of view. A 3-axis micropositioner (MMO-203, Narishige Group) was used to manipulate the sample holder and, therefore, the droplets/bubbles in the field of view. By this means, we were able to locate and manipulate droplets to stay on-screen throughout the test and track the resulting bubbles” (Sheeran, *et al.*, 2011).

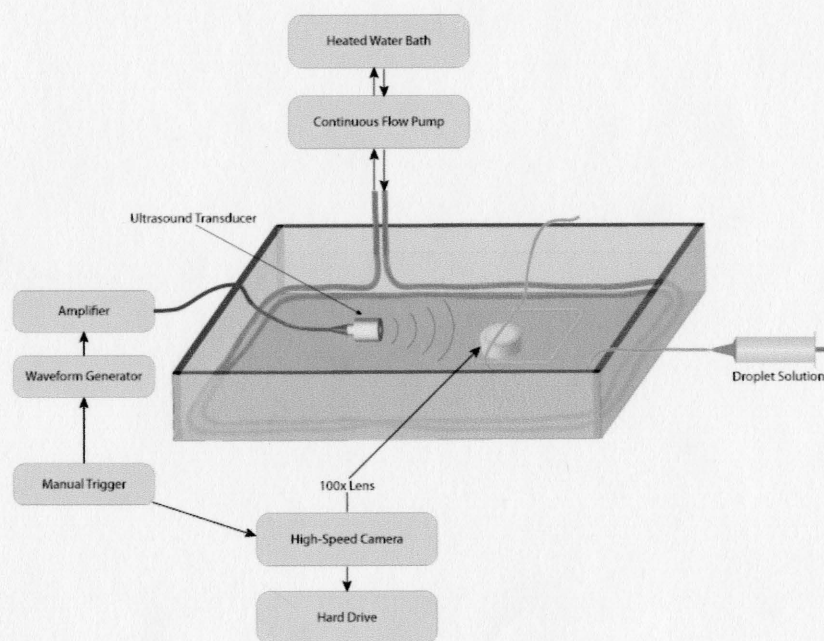


Figure 2.1. Experimental setup (unpublished figure courtesy of Sheeran, *et al.*, 2011). High-speed camera captured two-dimensional images of droplets and bubbles.

2.8. Acoustics

According to Sheeran and colleagues, “a spherically focused 5 MHz transducer with a focal length of 3.8 cm (IL0506HP, Valpey Fisher Corp., Hopkinton, MA, USA) was used to insonify droplet samples. The transducer had a -6 dB beam widths of 0.7 mm laterally and 13.2 mm axially for peak positive pressure, while widths were 1.3 mm laterally and 22.8 mm axially for peak negative pressure. Waveforms were constructed using an arbitrary waveform generator (AWG 2021, Tektronix, Inc., Beaverton, OR, USA), which allowed for adjustment of the transmission waveform pulse length and amplitude. Two manually-triggered signals of adjustable amplitude were used for these experiments: 1) a 10-cycle sinusoid at 5 MHz resulting in a total insonification time of 2 ms, and 2) a 10,000 cycle sinusoid at 5 MHz resulting in a total insonification time of 2 ms, following the results of Lo *et al.* (2007). A synchronization pulse from the waveform generator was relayed to the high-speed camera in order to trigger a marker with the acoustic pulse on the digital video. The waveform from the function generator was amplified approximately 60 dB using an RF amplifier (A500, ENI) in order to excite the transducer. For optical-acoustic alignment, the transducer focus was matched with the optical focus by positioning the tip of a needle hydrophone (HNA-0400, Onda Corp.) in center of the microscope field of view. The transducer was then calibrated at focus over the range of amplitudes used so that the pressure exerted on the droplets in the field of view was known” (Sheeran, *et al.*, 2011).

3. RESULTS

3.1. Storage Stability

The z-averages of each sample are plotted in Figures 3.1, 3.2, and 3.3 for storage temperatures of 4°C, 23°C, and 40°C, respectively. The samples stored at 4°C remained stable for the entire 16 weeks and did not deviate too far from their baseline z-average values. Not all of the samples had the same initial diameter (Figures 3.2 and 3.3) even though all homogenizations were performed with a 200 nm membrane filter. Perfluorocarbon droplets exhibited large deviations from baseline z-average values at 23°C and 40°C. Also, some samples evaporated at 23°C and 40°C where some data could not have been obtained. The corresponding raw data can be found in Appendix C.

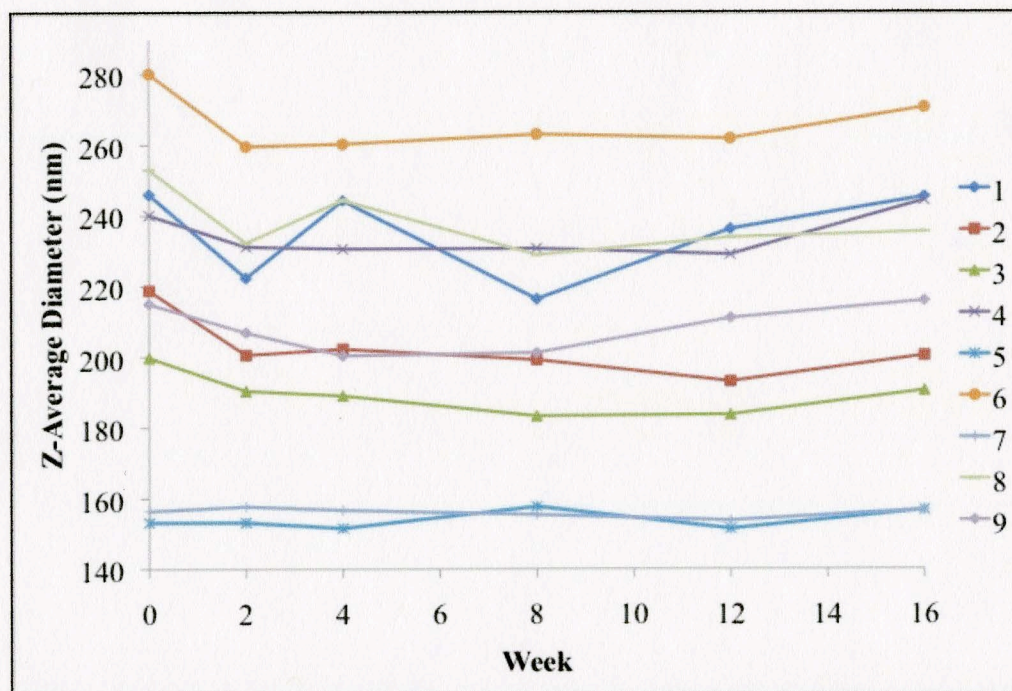


Figure 3.1. Z-averages for nine samples that were stored at 4°C and monitored for 16 weeks. Samples 1-3 are PFH droplets, samples 4-6 are PFMP droplets, and samples 7-9 are PFP droplets.

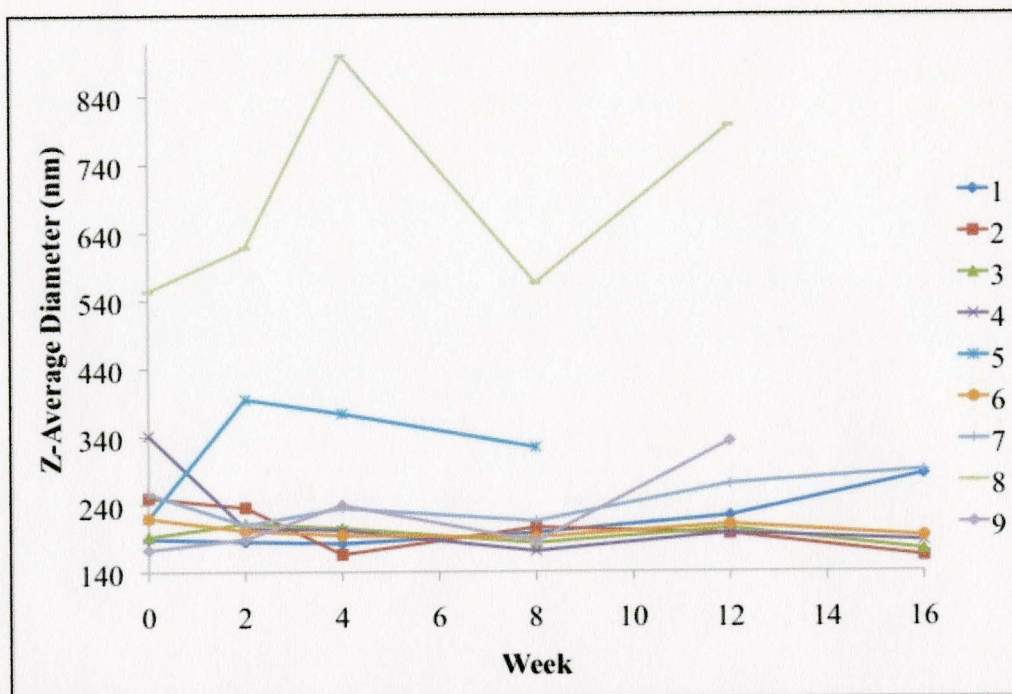


Figure 3.2. Z-averages for nine samples that were stored at 23°C and monitored for 16 weeks. Samples 1-3 are PFH droplets, samples 4-6 are PFMP droplets, and samples 7-9 are PFP droplets. Missing data points are due to errors with data acquisition and/or evaporation of sample.

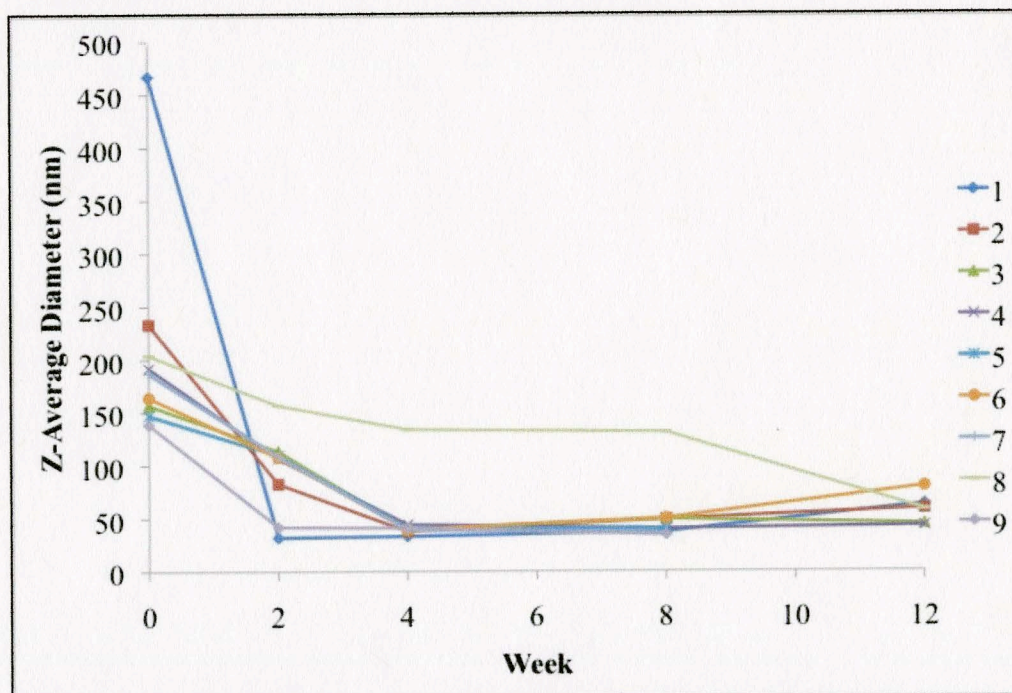


Figure 3.3. Z-averages for nine samples that were stored at 40°C and monitored for 12 weeks. Samples 1-3 are PFH droplets, samples 4-6 are PFMP droplets, and samples 7-9 are PFP droplets. Not enough sample was left for data acquisition at 16 weeks.

If the droplets maintained their z-average values within ten percent compared to the corresponding baseline z-average values, then the droplets were determined to be stable. Appendix C describes the method for how stability was determined. Figures 3.4, 3.5, and 3.6 show the deviation from baseline droplet sizes over a 16 week period at 4°C, 25°C, and 40°C, respectively. The error bars are large because they represent the standard deviation of three individual samples that may vary in z-average size. The average deviation of the droplets was less than ten percent from the baseline values at 4°C and throughout most of the test period for 23°C. PFH droplets were the least stable compared to the other droplets at 4°C. At 23°C, PFMP droplets deviated a little over ten percent after the first two weeks but later stabilized closer to baseline values and evaporated after 12 weeks. PFP droplets had deviated 31% and 47% away from baseline z-average values at weeks 4 and 12, respectively, but they were near baseline values at week 8 when stored at 23°C.

Moreover, most of the droplets were far from their baseline values after the first two weeks at 40°C. Specifically, the z-average values were smaller compared to baseline values. This suggests that evaporation of the perfluorocarbons occurred after the first two weeks, and there was potential self-assembly of liposomes of smaller sizes. Thus, the data suggests greater stability at cooler temperatures.

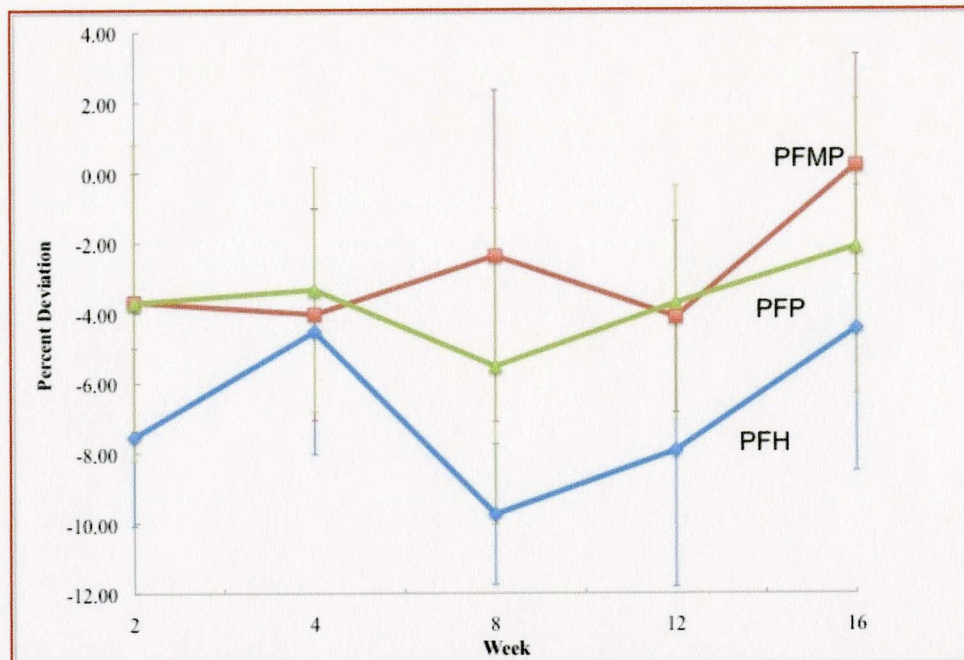


Figure 3.4. Average percent deviations of each group of perfluorocarbon droplets compared to week 0 at 4°C. Average percent deviations were no greater than 10% from original sizes over 16-week period. Error bars are large because they represent the standard deviation of 3 samples that vary in z-average size ($p = 0.01$).

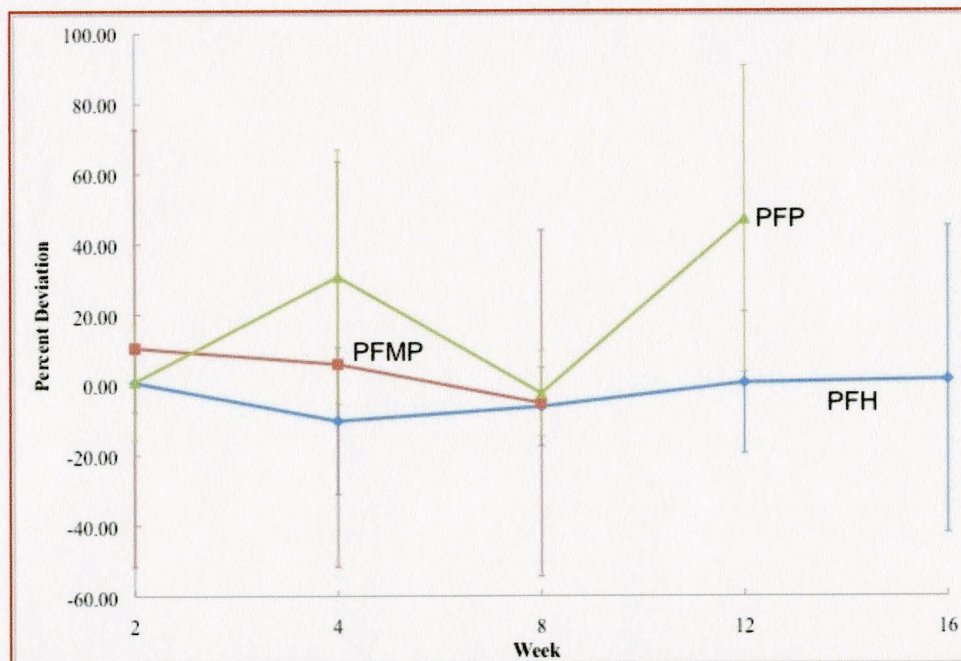


Figure 3.5. Average percent deviations of each group of perfluorocarbon droplets compared to week 0 at 23°C. Droplets were monitored over 16-week period. Missing data points due to evaporation of samples. Error bars are large because they represent the standard deviation of 3 samples that vary in z-average size ($p = 0.14$).

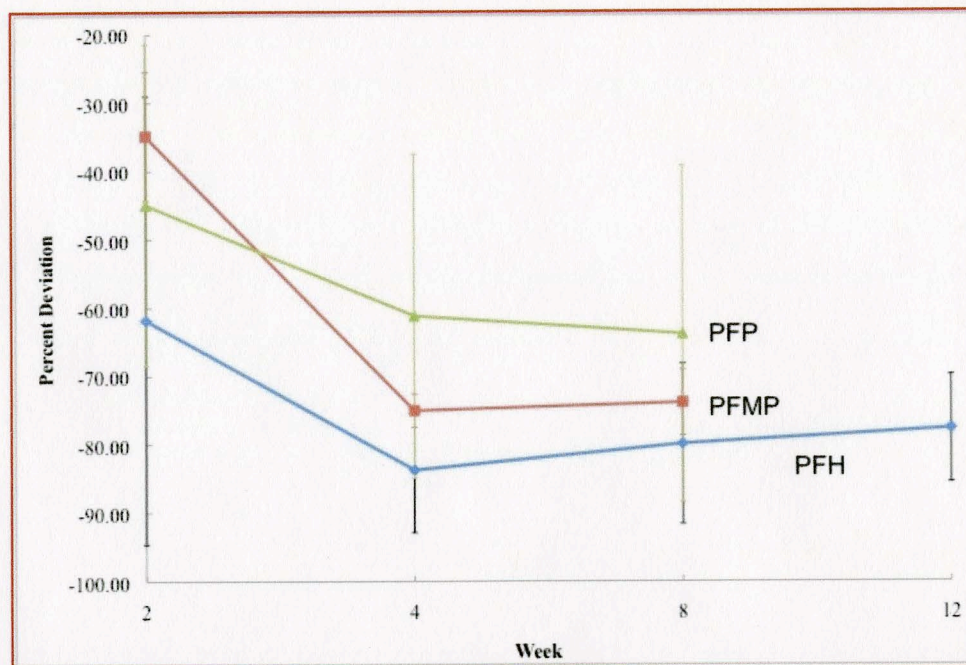


Figure 3.6. Average percent deviations of each group of perfluorocarbons compared to week 0 at 40°C. Droplets were monitored over 12-week period. Missing data points due to evaporation of samples. Error bars are large because they represent the standard deviation of 3 samples that vary in z-average size ($p = 0.26$).

Figures 3.7, 3.8, and 3.9 show the size distributions by intensity obtained from the particle size analyzer of perfluorohexane droplets. Figures 3.7 and 3.9 show that the baseline size distributions were bimodal. This suggests that not all of the samples can be reproduced with uniform distributions with the methods performed. In general, the size distribution for the PFH droplet sample at 4°C (Figure 3.7) remained the same although PFH droplets were the least stable compared to the other droplets at that temperature. However, Figures 3.8 and 3.9 show that the samples did consequently become unimodal after 16 weeks. The size distributions shown in Figures 3.8 and 3.9 also exhibit the average sizes of the droplets becoming smaller.

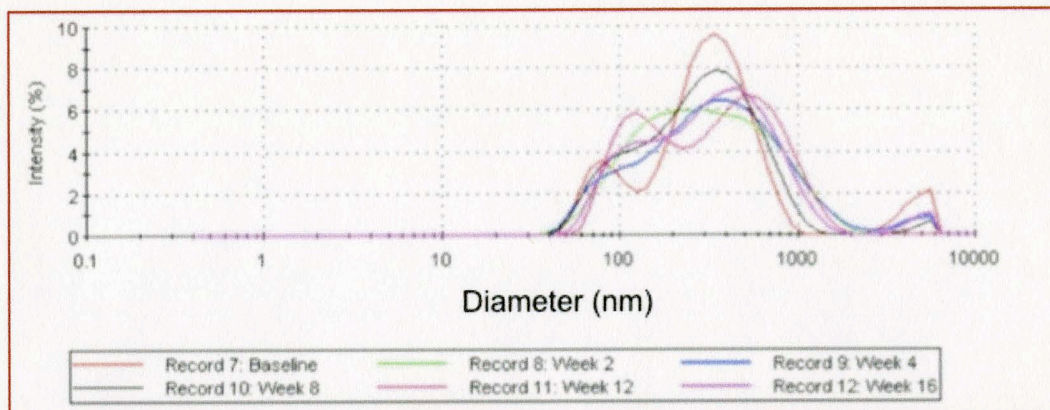


Figure 3.7. Size distributions by intensity of perfluorohexane sample stored in 4°C for 16 weeks. Size distribution was bimodal for week 0 and week 16 suggesting a nonuniform sample but still maintained relatively the same size distribution. 4°C is ideal for storage of droplets.

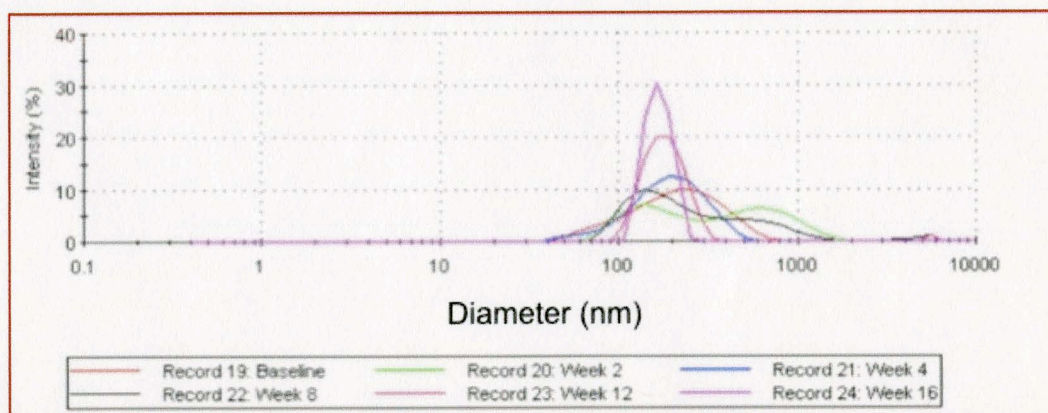


Figure 3.8. Size distributions by intensity of perfluorohexane sample stored in 23°C for 16 weeks. Size distributions shifted slightly to the left over time suggesting that majority of the droplets became smaller. The size distribution was more steep at week 16 suggesting a more uniform distribution.

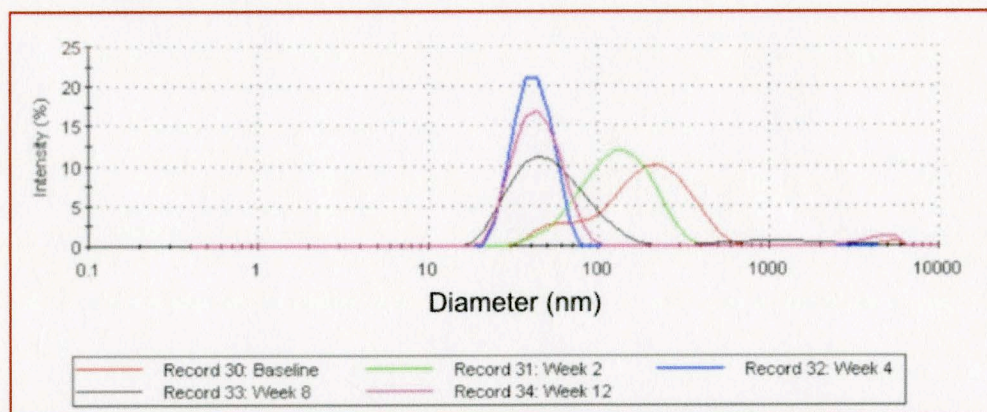


Figure 3.9. Size distributions by intensity of perfluorohexane sample stored in 40°C for 12 weeks. No data was obtained for week 16 due to evaporation of samples. Size distributions shifted to left suggesting droplets became smaller over time.

3.2. Acoustic Droplet Vaporization (ADV)

PFC droplets were sent to UNC for ADV tests, which is also where data was collected and analyzed by Sheeran and colleagues. PFH droplets were observed to not be able to vaporize at all test parameters of ultrasound output energy. This inherent stability of PFH is attributed to its high boiling point and the stability of the outer shell of the PFH droplets. On the other hand, the other perfluorocarbons were able to vaporize. Figure 3.10 shows vaporization thresholds (MIs) as a function of diameter. PFB droplets required less MI, which translates to requiring less ultrasound output energy, than PFP and PFMP droplets in order to vaporize. The larger droplets required less MI than smaller droplets, which was similar to other reported results (Kripfgans, *et al.*, 2004). The raw data was extrapolated beyond the range of the collected data, especially for PFP and PFB droplets, which should not have happened. Also, for the fit for PFMP, there appears to be a significant drop-off beyond 21 μm .

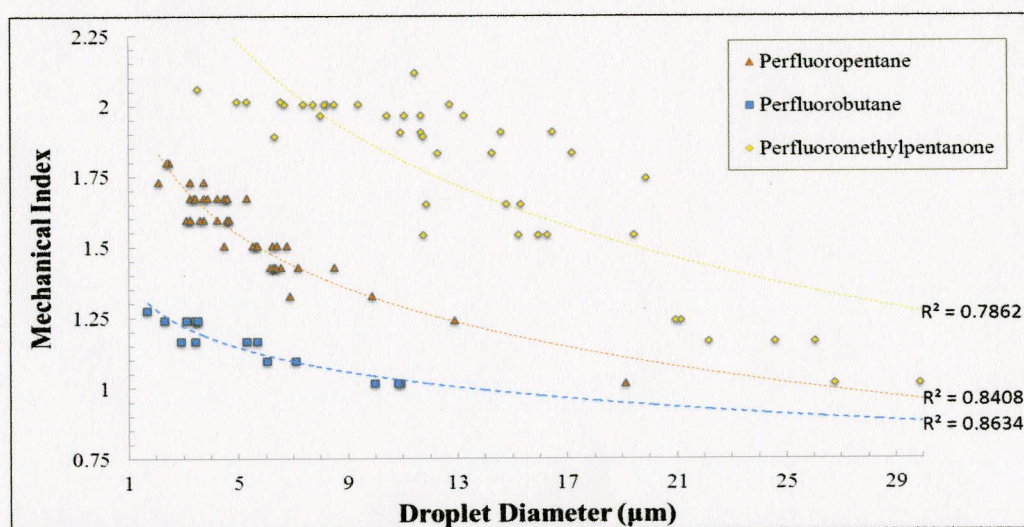


Figure 3.10. Mechanical Index versus initial droplet diameter. Each droplet diameter required a specific MI in order to become vaporized (vaporization thresholds). PFB required less ultrasound output energy than PFP and PFMP. Each tick mark on mechanical index scale represent five hundredths.

Stable droplets were isolated and recorded for set pulse lengths of 2 μ s or 2 ms. Figure 3.11a shows still images of an isolated stable droplet that later became a bubble after ADV. Immediately after application of ultrasound output, PFP and PFB droplets showed an increase in diameter by an average factor of 10.39 ± 2.27 in solution that had not been degassed within the allotted pulse length times (Figure 3.12). The bubbles in solution that had not been degassed continued to grow an average of 21.9% of their original bubble diameter (taken at final pulse length). When the solution was degassed, droplet diameters increased by an average factor of 6.24 ± 0.58 , and those bubbles continued to grow an average of 3.6% of their original observed diameters (also taken at final pulse length). This is closer to the estimated calculated value from the ideal gas law, which suggests that the droplets should increase between 5 and 5.5 times their original diameters. Volume was not monitored nor recorded directly due to the limitations of the experimental setup; therefore, it was easier to identify a diameter with the two-dimensional images that were acquired. Moreover, the greater increase in size in solution that had not been degassed suggests that perfluorocarbons have the innate ability to absorb excess gas in its environment (see Section 4.2), which is also dependent on the concentration of the excess gases in the environment.

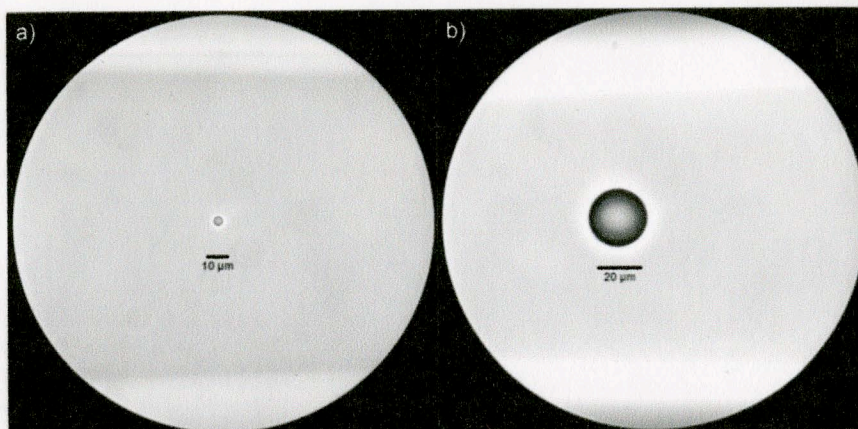


Figure 3.11. Before and after pictures of an isolated and stable PFB droplet. a) PFB droplet is roughly 5 μm in diameter. b) PFB droplet becomes a 20 μm in diameter bubble after acoustic droplet vaporization (ADV).

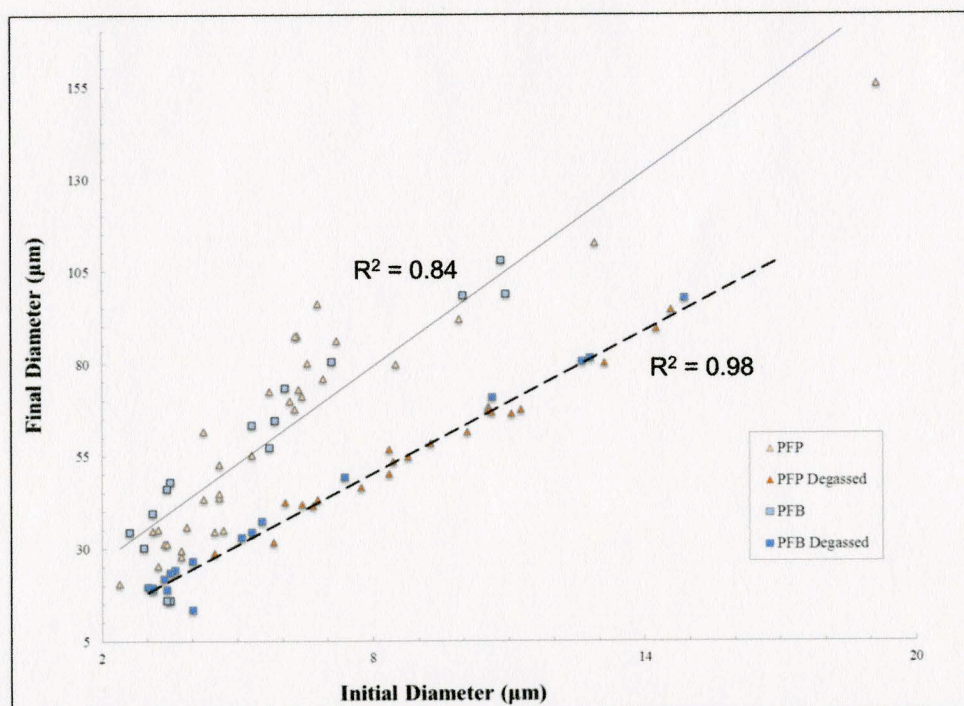


Figure 3.12. Relationship between initial and final diameters in solution for PFCs with boiling points less than 37°C. The trends are consistent and not dependent on PFC type. Degassed solution exhibited an increase by a factor of 6.24 ± 0.58 while solution that had not been degassed exhibited increases by a factor of 10.39 ± 2.27 from the original diameter.

For PFC droplets with boiling points greater than normal body temperature (37°C), PFH did not vaporize under the experimental conditions. On the other hand, PFMP did

vaporize but did not show any differences when vaporized in degassed and undegassed solutions (Figure 3.13). While the experimental conditions and data acquisitions were similar as those done for PFP and PFB, there was a spot in the nuclei of the droplets. This suggests that the nuclei were just entering the gaseous phase, and full expansion of droplets did not occur until much later after ultrasonic power was applied.

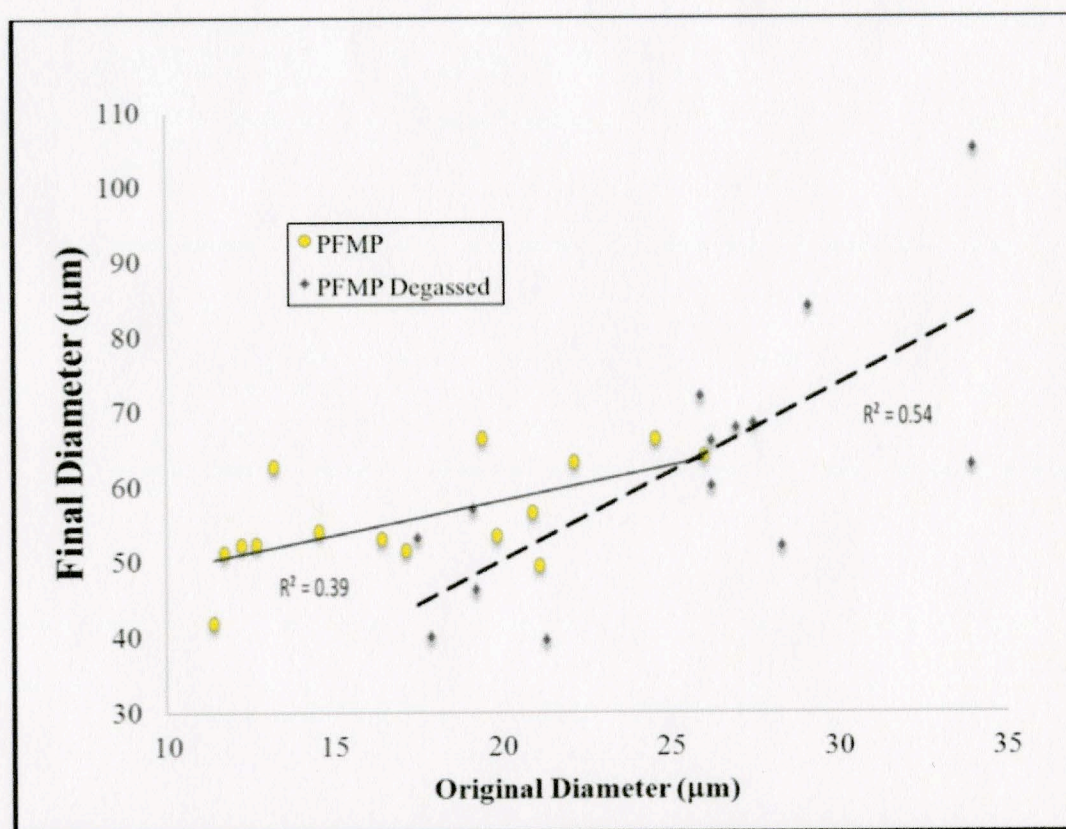


Figure 3.13. Relationship between initial and final diameters in solution for PFMP droplets. PFMP droplets did not fully vaporize at final pulse length measurement.

3.3. Encapsulation of Perfluorobutane

Initial attempts were made to encapsulate liquid PFB inside a lipid membrane. The first attempt involved the use of the Avanti Mini-Extruder after adding PFB to the lipid solution at room temperature (23°C). Extrusion was deemed impossible because most of

the PFB had vaporized upon addition to the lipid solution. Therefore, the next attempt involved insertion of the lipid solution into the PFB glass vial followed by shaking on the “dental shaker”. There were two liquid layers because a pressure head containing “excess” PFB gas may have formed. Therefore, efforts were made to capture the size of PFP (Appendix D) and PFB droplets via SEM, TEM, and dynamic light scattering. It was expected to see the nanodroplets as spherical structures; however, the structures of the perfluorobutane sample appeared as holes in SEM images (Figure 3.14a), which were verified by the EDS in addition to tilting the sample (Figure 3.15a). The fluorine detection from the EDS for the PFB sample showed that the fluorine had dispersed into the web-like structure that had formed as a result of the air-drying process for SEM sample preparation in addition to the nature of the perfluorocarbon (Figure 3.15b). However, the results appear equivocal considering the boiling point of the PFB and the isolation process of the droplets.

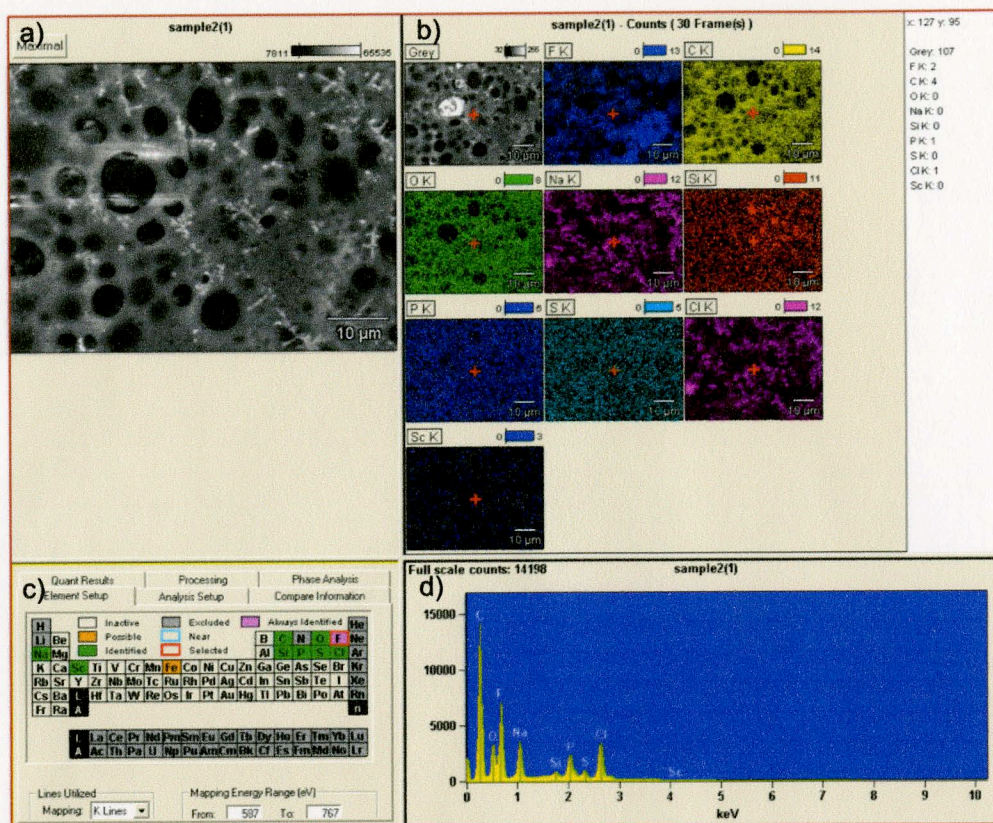


Figure 3.14. Screenshot of computer software interface containing a) SEM image and b) EDS result obtained for PFB droplet sample. c) Periodic table of elements showing which have been identified. d) EDS spectra. Fluorine peak is indicative of presence of PFB.

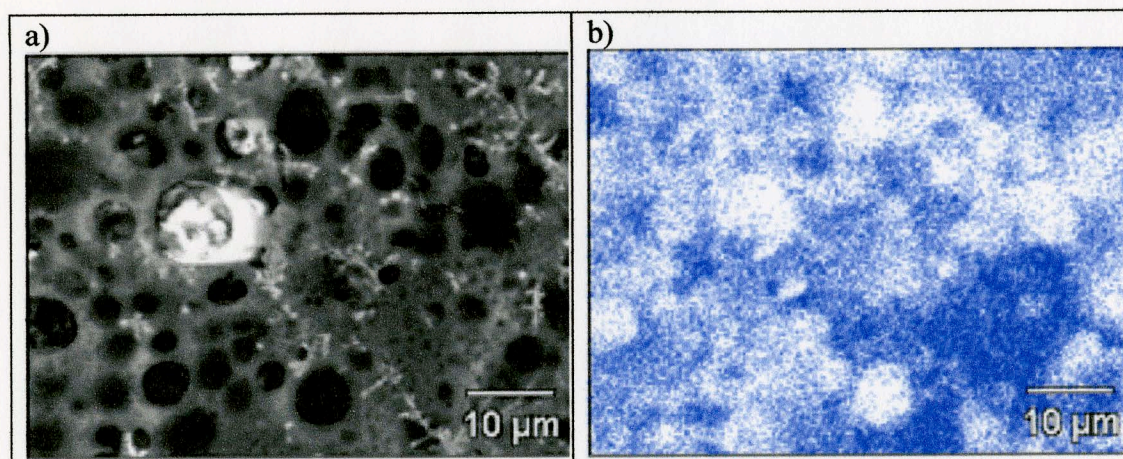


Figure 3.15. SEM and EDS results of PFB sample. a) PFB sample tilted highlighting perimeters of holes. b) EDS of perfluorobutane sample showing dispersion of fluorine (blue content) in web-like structure.

As demonstrated by a TEM image of PFB droplets (~100 nm) prepared at room temperature (25°C), the membrane structures of the PFB sample appear to be thick and most likely have more than one layer (Figure 3.16). It is unclear as to whether or not this is representative of the actual PFB droplets or if they are bubbles as a result of their natural tendency to vaporize.

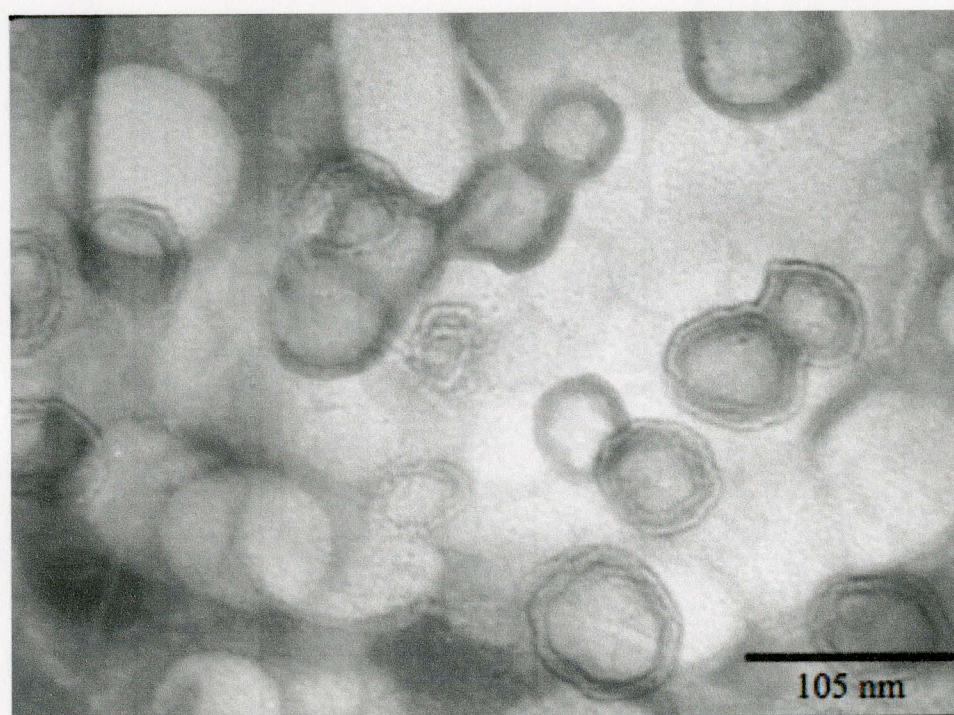


Figure 3.16. TEM image of PFB droplet sample prepared at room temperature. Membranes appear to have more than one layer.

The population of PFB droplets (Figure 3.16) was not distributed throughout the entire TEM grid and was recognized as not being a uniform sample. Also, PFB droplets vaporized immediately at room temperature; therefore, PFB droplets were prepared for analysis via freeze-fracture TEM (Figure 3.17). The droplets are between 20 and 40 nm in diameter. However, such droplets would not work for ultrasound imaging because the droplets would then result in approximately 200 nm diameter bubbles that are too

difficult to visualize with ultrasound imaging because of their size and their likelihood to rapidly collapse due to Laplace pressure. These particles are more likely to be lipid particulates remaining after extrusion.

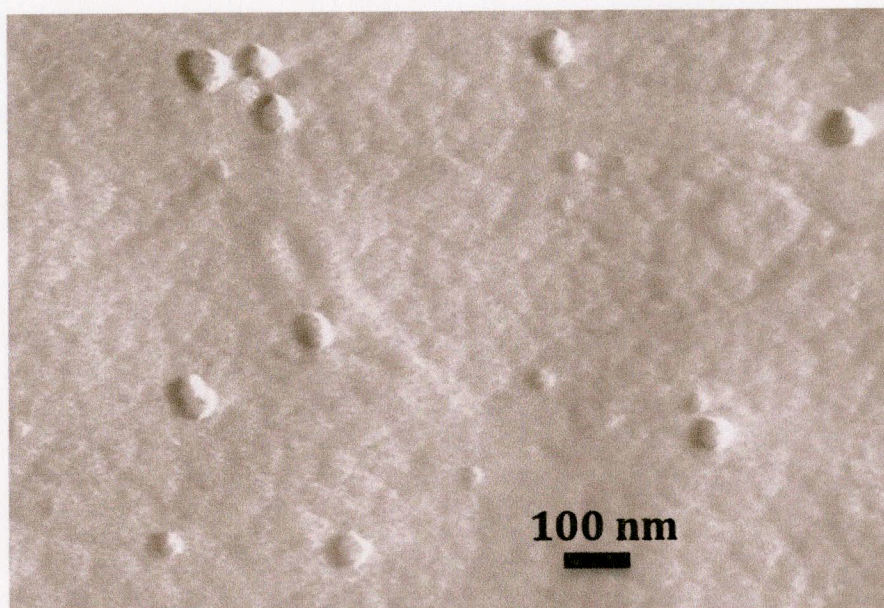


Figure 3.17. Freeze-fracture TEM image of putative PFB droplets. They are 20-40 nm in the background.

It was impossible to obtain a precise measurement reading from the dynamic light scattering for PFB droplets because the sample was too polydisperse suggesting that the PFB droplets were not uniform in size after preparation for the particle size analyzer. Therefore, the PFB droplets were then further stabilized with lipids and glycerol for ADV experiments. Fluorine content could not be detected after SEM preparation of these new droplets, and no clear or defined structures of droplets were found with TEM.

4. DISCUSSION

Perfluorocarbon droplets were investigated in terms of storage stability, formulations, and vaporization.

4.1. Storage Stability of Perfluorocarbon Droplets

The shelf-life stability of perfluorocarbon droplets is important because it is necessary to identify how long this formulation could potentially be stored after preparation should this type of formulation become a diagnostic or pharmaceutical tool. The droplets were more stable in a 4°C environment with an average deviation of less than 10 percent from the baseline values. Therefore, the droplets should be stored at 4°C prior to testing. Temperatures above 4°C increase risks for droplet degradation, aggregation, or coalescence. There appeared to be no relationship between boiling point and stability, although PFH droplets were the least stable at 4°C and 40°C while PFMP droplets were the least stable at room temperature (23°C).

The size distributions based on the light scattering intensity of the perfluorocarbon droplets varied over time at the three temperature settings. This variation in distribution may be a result of aggregation and coalescence of the droplets (Ostwald ripening) (Basude, *et al.*, 2000). In addition, the distributions were based on intensity, and the intensity-weighted scattering of the particle sizer is proportional to the diameter of the droplet raised to the sixth power. Therefore, one large particle/droplet can skew the size profiles. Nonetheless, the distribution of droplets remained roughly the same at 4°C suggesting that such an environment provides more stability. The distribution of droplets became more uniform over time at 23°C and 40°C. Also, the

interactions between the lipids, perfluorocarbons, and HEPES buffer may stabilize to a favorable state of uniformity on their own. Although the samples were capped, this still may be the result of evaporation of the samples, as they lost volume over time. The perfluorocarbons may have evaporated before water because of their lower boiling points. The evaporation of perfluorocarbon may have left the lipids to spontaneously form liposomes of uniform size. It is also possible that the particle size detector may have detected smaller droplets more frequently than larger sized droplets.

4.2. Vaporization Thresholds of Perfluorocarbon Droplets

Perfluorocarbon droplet samples were subjected to vaporization testing. PFMP, PFP, and PFB droplets vaporized with the set experimental parameters while PFH droplets did not vaporize due to having higher vaporization thresholds. PFP and PFB droplets were able to vaporize with mechanical indices less than the FDA accepted maximum clinical setting ($MI = 1.9$) (Figure 3.10). However, the visualized droplets were greater than $1\ \mu\text{m}$ in diameter, and the desired $200\ \text{nm}$ droplets were not easily visible. The ultrasonic energy might not only provide thermal energy, but it might also provide mechanical energy such that the droplets and/or bubbles might aggregate and coalesce to form larger droplets/bubbles, also known as Ostwald ripening (Rapoport, *et al.*, 2007). This may result in further stabilization of some of the droplets/bubbles. In addition, the mechanical energy might cause the membranes to oscillate and eventually undergo inertial cavitation where the bubbles would collapse, especially affecting smaller bubbles.

From the ADV experiments, it appears that vaporization factors include the surrounding environment (gases in solution), the droplet sizes, and acoustic output. If there is gas present in the surrounding environment, the perfluorocarbons may have a tendency to absorb the gas, which would produce much larger bubbles than calculated from the ideal gas laws. The absorption of environmental gases is not surprising because perfluorocarbon liquids have been used as oxygen carriers for blood substitutes (Biro, *et al.*, 1987 and Spahn, *et al.*, 1994). For future *in vivo* experiments, the amount of excess gas would definitely be variable, and the perfluorocarbon droplets may expand similar to their expansion in solution that had not been degassed. Also, larger droplets had lower vaporization thresholds than smaller droplets because they may have had lower vapor temperatures as predicted. Therefore, the required thermal energy was greater for smaller droplets as they may have simultaneously coalesced to form larger droplets/bubbles upon heating (Gao, *et al.*, 2008 and Rapoport, *et al.*, 2007). While smaller bubbles (750 nm to 1 μm in diameter) would derive from smaller droplets (150 nm to 200 nm in diameter), their higher vaporization thresholds might also derive from having less perfluorocarbon content, which would in turn result in absorption of less gas. The amount of perfluorocarbon contained in the droplet is relative to the droplet size, and heating of perfluorocarbon would produce bubbles of relative size that are about 5.5 times larger in diameter than the original droplet diameter as a result of non-inertial cavitation.

The results from this work imply that it is possible to stabilize perfluorocarbon liquid within membrane shells. Although the perfluorobutane liquid required further stabilization with glycerol, the properties of the droplets were not impacted such that

lower MIs were required to vaporize the PFB droplets. Even though this may appear to be very promising in the design of a probubble that could eventually become an extravascular agent, the MIs used in the experiments especially for PFMP and PFP were near the upper range of MIs used in the clinical setting (Figure 3.10). While the droplets tested were greater than 1 μm in diameter due to the optical limitations provided by the microscope, this also suggests that smaller droplets may require much higher MIs, which would most definitely be at risk for potential bioeffects *in vivo*. Therefore, encapsulation of lower boiling perfluorocarbons may need to be further explored.

The increase in sizes was much greater for gassed solutions compared to degassed solutions (Figure 3.12). This difference is due to the nature of perfluorocarbons and their ability to absorb excess gases in their surrounding environments. For comparison, the average increase for the droplets in degassed solution was 6.24 ± 0.58 times the initial droplet size, which is very close to the calculated conversion of 5-5.5 times the droplet size according to ideal gas law calculations (Appendix A). Although the increase is still higher than the calculated factor, this may suggest that the solution was not entirely degassed and/or the smaller bubbles had aggregated and coalesced. A solution that is not degassed is representative of physiological conditions. Typically, it appears that the amount of oxygenation near a tumor site is dependent on the stage of the tumor where newer tumors tend to have more oxygenation due to neovascularization, and older malignant tumors are often hypoxic (Vaupal, *et al.*, 1989). However, newer tumors might have hypoxic microenvironments, thus the surrounding environments near tumors remain unknown because of the constant changes that cancer can undergo.

Nevertheless, the increase in sizes from degassed solution can be used to estimate the initial droplet sizes. For example, a 30 μm diameter bubble would most likely have derived from a 5.5 μm droplet. The increase in size in degassed liquid suggests that the perfluorocarbons load excess gases spontaneously and rapidly. Perfluorocarbons do not necessarily react with the excess gases but rather only draw them into the droplets/bubbles, and thus, there exists a mixture of perfluorocarbons and other gases (oxygen, nitrogen, carbon dioxide). Hence, the average increase in bubble size is a little more than the theoretical value whereas the microbubble conversion in undegassed solution would be much greater due to absorption of more excess gas. Meanwhile, the perfluorocarbon content is probably maintaining the structural integrity of the bubbles because most air bubbles tend to collapse much more quickly than perfluorocarbon bubbles (Porter and Xie 1995). Other potential factors that may affect the expansion of the droplet to a bubble are the pressure and the surface tension.

Furthermore, PFMP droplets converted to final bubble diameters tens of seconds later than PFP and PFB droplets. The nuclei of the droplets appeared to have had two phases (liquid and gas) suggesting the genesis of microbubbles. Hence, the state of the nuclei of the droplets/bubbles and the percentage of that state could determine how much excess gas the perfluorocarbon could absorb. In addition, this rate of conversion to gas could potentially lead to exploring higher boiling perfluorocarbons and determining the parameters to vaporize perfluorocarbons. A slower rate of data acquisition may be necessary for these studies than the acquisition rates that are currently available.

4.3. *Perfluorobutane Encapsulation*

Stable PFB droplets were formulated by using lipids, and they withstood temperatures up to 37°C. Encapsulation of PFB had to be conducted under pressure or at temperatures below the boiling point of PFB. However, the sizes of the PFB droplets were difficult to confirm via TEM or submicron particle sizing because the PFB droplets foamed upon insertion of a needle in order to extract some sample. TEM results (Figure 3.16) remain equivocal as to whether or not PFB droplets were capable of being imaged. Accurate particle sizing was impossible because particle size analysis suggested that the sample was too polydisperse.

Consequently, glycerol was added to the PFB droplet formulation, which resulted in a more stable solution that did not foam upon insertion of a needle to obtain some sample. The glycerol prevented PFB droplets from instantaneously vaporizing when attempting to draw out the sample. Adding glycerol may have also increased the vapor temperature for PFB by providing a more solid membrane, which makes it more relevant to the Laplace pressure estimation. However, it remained difficult to assess PFB droplets with TEM. The particle size analysis provided the same polydisperse result. Further investigations of methods of identifying and visualizing these types of droplets may be necessary.

5. CONCLUSIONS

5.1. Conclusions on Storage Stability of Droplets

The study demonstrated that the storage stability of perfluorocarbon droplets is not dependent on boiling point but is dependent on temperature storage conditions. It is important to keep the perfluorocarbon droplets refrigerated prior to use in ultrasound-mediated applications. Droplets less than 1 μm in diameter can be made with the methods used in this study. Nonetheless, methods of developing a more uniform sample of perfluorocarbon-filled droplets need to be further investigated. Better containment of samples in future storage stability studies may be necessary to prevent evaporation of samples.

5.2. Conclusions on Vaporization Thresholds

Four different types of perfluorocarbons were explored in order to investigate their vaporization thresholds as droplets. PFH droplets are not appropriate droplets for ultrasound-mediated applications because they require much greater energy for vaporization and will cause greater risk for potential bioeffects. PFB droplets may require ultrasound energy output within clinical ranges. Higher ultrasound energy output is required as droplet size decreases below 1 μm in diameter. Encapsulation of lower boiling perfluorocarbons may be necessary to use reasonable MIs for droplets 200 nm in diameter. Other methods for isolating and viewing smaller droplets need to be explored.

5.3. Conclusions on Encapsulation of Perfluorobutane

The SEM and TEM images of perfluorobutane droplets were not able to confirm encapsulation of liquid PFB into a lipid membrane. However, further stabilization with

another substance, such as glycerol, prolonged the lifetime of PFB droplets prior to ADV, which confirmed the stabilization of PFB droplets.

6. FUTURE STUDIES

While the ultimate goal is to design a probubble that will begin as a droplet and vaporize into a microbubble using ultrasound, some details are still necessary to investigate. Some of these details include optimization of various steps in the process:

- A. One of the main methods that need to be investigated is the ability to obtain more uniform droplets. There are a number of parameters that can affect the distribution of droplets after homogenization, including the lipid composition, lipid concentration, perfluorocarbon concentration, type of membrane used during homogenization, number of passes through membrane, amount of pressure during homogenization, and rate of extrusion. The variation of membrane concentration to perfluorocarbon concentration has been investigated before (Gao, *et al.*, 2008) but with biodegradable block copolymers. To eliminate the potential for human error during extrusion, Avestin has a pneumatic actuator (Ottawa, Canada) that is capable of performing the extrusion semi-automatically thereby controlling the amount of shear stress imposed upon the formation of droplets and existing droplets. However, a uniform sample of droplets greater than 200 nm may not be possible to fabricate via membrane extrusion. This is important because we want to know the initial nonvisible droplet size that would correspond to its final visible bubble. With the exception of other researchers (Lo, *et al.*, 2007 and Giesecke and Hynynen 2003) who use a similar device to the Avanti Mini-Extruder (Liposofast), it appears that other groups obtain their uniform droplets via emulsification through a microfluidizer (Fan, *et al.*, 2006 and Schad and Hynynen 2010) or simple sonication in a water bath (Rapoport, *et al.*,

2009). The potential problem with testing another device is the required capability of investigating lower boiling perfluorocarbons.

- B. Further investigation of stabilization of PFB droplets remains necessary to determine the best encapsulating method that would allow for lower MIs to be used to cavitate droplets. Even though glycerol provided enough stability for PFB droplets to perform ADV tests, it was impossible to monitor the size of the droplets using particle size analysis because samples were too polydisperse. Therefore, another stabilizer such as layer-by-layer assembly (Borden, *et al.*, 2007) could be applied where shells of charged polymers “wrap” around the shells of the lipid membranes. The current membrane contains a polyethylene glycol tail that is pointed away from the droplet core and is slightly negatively charged. This negative charge can be a potential linker for a number of items including oppositely charged polymers, proteins, and monoclonal antibodies. Also, it may be possible to visualize smaller bubbles because the charges can be labeled with fluorescent dyes or other markers. Thus, the limitation for experimentation is the ability to visualize such small droplets, which should be tackled in future studies.

Another potential method to investigate for stabilizing lower boiling perfluorocarbon droplets would be a mixture of perfluorocarbons. This had been done briefly with varying ratios of 2H,3H-perfluoropentane (BP = 55°C, Chemical Book 2008a) to perfluoropentane where an increase in the ratio resulted in an increase in vaporization threshold (Kawabata, *et al.*, 2005).

- C. This research would be accelerated with an apparatus that can liquefy low-boiling perfluorocarbons or hydrofluorocarbons at a rate that would be convenient for droplet formulation. This apparatus should be able to take nearly any perfluorocarbon or hydrofluorocarbon that is vapor at room temperature and condense it into liquid form. The amount of liquid produced would be known and kept inside a capped and crimped glass vial stored at -20°C . While the vapor temperature theory (section 1.7.2) suggests that perfluoropropane (boiling point = -36.7°C , Linstrom and Mallard 2010) can be encapsulated in a membrane and have an increased vapor temperature of 35°C , the perfluorocarbons used within this apparatus must not have a vapor temperature less than -36.7°C and no more than room temperature (23°C). Homogenization processes typically take about 10 minutes when all material (lipids, cryoprotectant, and perfluorocarbon) are ready; therefore, the perfluorocarbons must liquefy within 5-10 minutes prior to homogenization, and homogenizations must occur at -20°C .
- D. Other imaging techniques for identification of droplet sizes may need to be approached. There exists a gravity-driven microfluidic particle sorting device that is capable of separating perfluorocarbon droplets that are about $1\ \mu\text{m}$ or greater in diameter (Huh, *et al.*, 2007). Such a device could be used to identify submicron droplets via an oil-immersion technique using a basic upright microscope. However, sub-microchannels would need to be used in addition to microchannels to route and visualize the droplets. Because there will always be a population of various sizes of

droplets and not necessarily a uniform sample, this device could assist in producing a more uniform sample.

- E. Another method of viewing smaller droplets, or even bubbles, would be necessary in order to accurately confirm the theoretical calculations of bubble expansion before and during ADV. Smaller droplets must be investigated to facilitate extravasation into the extravascular space. One possible method would be to isolate one droplet by attaching an optical dye and a ligand to the membrane. There will be a corresponding receptor that recognizes the ligand in agarose gel. Viewing may be done via noncontact atomic force microscopy (AFM), which can be performed for wet samples.

On a similar note, the phenomena of Ostwald ripening needs to be confirmed with instruments that have high optical resolution as well as possibly with fluorescent tags attached either to the lipid membranes or the internal core. Such an instrument could potentially be used to further confirm not only the presence of perfluorocarbon droplets but also true encapsulation of perfluorocarbon within a droplet even though a whole population of droplets may be within the field of view. A very small sample of droplets between 100 and 200 nm in diameter must be isolated and tagged to see if such aggregation and coalescence would occur. Along with a potential fluorescent tag on either the lipid membrane or the internal core, an oil immersion microscope with epi-fluorescence illumination could be used with a charge-coupled device (CCD) camera to capture the small droplets. The droplets would be isolated via filtration.

- F. While the tested droplets were larger than 1 μm in diameter, it remains necessary to develop smaller droplets that can extravasate to the extravascular space. The requirements for extravasation of these droplets might be varying diameters, lipid compositions, and outer membrane components (PEG lengths, charges, and ligands). Potential imaging of PFB droplets and even other PFC droplets via MRI may be beneficial to further confirm extravasation. In addition, MRI may be used to detect migration of PFC droplets into cells. This has been demonstrated by detecting fluorine-19 (^{19}F) in nanoemulsions as they migrated into T cells (Janjic, *et al.*, 2008). Perfluorocarbon emulsions with ^{19}F have also been detected in rodent mammary tumors (Fan, *et al.*, 2006). It is also possible to detect ^{19}F nanoparticles to quantify angiogenesis (Water, *et al.*, 2008). However, these methods with ^{19}F MRI can be modified to determine the extravasation of PFC droplets after washouts.
- G. Another test group could involve isolated 100-200 nm droplets with ligands bound to corresponding receptors in a sol-gel glass matrix (Narang, *et al.*, 1993). Such a ligand could potentially be attached to the droplets and specific droplets could be monitored during ADV testing to determine if single droplets can indeed cavitate into microbubbles. All experiments should be done in undegassed and degassed solutions at 37°C and atmospheric pressure. The same ultrasonic parameters should be applied.
- H. Investigations of cell internalizations of droplets need to be performed to study receptor specificity and nonspecific endocytosis. Therefore, methods of attaching certain ligands should be investigated in addition to determine which ligands might be appropriate for this diagnostic and/or therapeutic tool. Most of the ^{19}F studies

mentioned earlier targeted specific cells. For example, one group incorporated a peptide ligand that recognizes the $\alpha_v\beta_3$ integrin onto their ^{19}F nanoparticles to detect potential angiogenesis pertinent to atherosclerosis or aortic valve stenosis (Waters, *et al.*, 2008). In addition, another group incorporated biotin to the membranes of some PFC ultrasound contrast agents to detect thrombi through a biotin-avidin system (Lanza, *et al.*, 1997). Although these examples are restricted to the vasculature, similar methodologies could be involved when attaching a ligand to the membrane of a droplet.

- I. Other ultrasonic parameters not related to the MI need to be further investigated because MI is not a useful factor in determining potential bioeffects (Forsberg, *et al.*, 2005). MI is only limited to the peak negative pressure and the center frequency. Other parameters include TI (acoustic output [W/cm^2] and energy required to raise tissue temperature 1°C), pulse length, and exposure time. In addition, if these parameters are known, boundaries can then be set and applied for future experiments.
- J. Various *in vivo* time points are necessary to note to determine how the probubble will function. For example, it is necessary to identify how long it will take for the probubble to accumulate within tumor cells, especially after physiological washout, as well as how long it will take for the probubble to be cleared out of the body. Therefore, small animal models with tumors can be used for these investigations along with the appropriate ultrasound equipment for probubble functionality and visual cues.

K. Certainly, the probubble could potentially be used for other biomedical applications not limited to detecting and intoxicating tumors. For example, it had been proposed to use such a device for tissue occlusion therapy to cauterize blood vessels near tumor sites in addition to correcting any phase aberrations (Kripfgans, *et al.*, 2000). Microbubbles improve contrast and highlight delineations within the region of interest on the ultrasound image. Therefore, the probubble can generally be used with nearly any ultrasound application where it may be difficult to view certain characteristics whether they may be particular to certain organs or even cellular structures.

APPENDIX A: SPREADSHEET OF PERFLUOROCARBON DROPLET
CALCULATIONS

Table 1.3 contains the physical properties of the perfluorocarbons used in these experiments. Below are the results from an Excel spreadsheet indicating the calculations involved in determining the final bubble size from the initial droplet size.

	A	B	C	D	E	F	G	H
◇								
1	Droplet Diameter (nm)	200	$r = d/2$		P (atm)	1		
2	Volume (nm³)	4.19E+06	$V = (4/3)\pi(r^3)$		Vbubble (L) = nRT/P			
3	Volume (mL)	4.19E-15	$mL = 10^{21} \text{ nm}^3$		n (mol) = Vdroplet * Liquid Density / MW			
4					R (L*atm/mol*K)	0.0821		
5					T (K)	310.13		
6								
7	Bubble diameter (nm) = ((Vbubble(L)*1000mL/L*(10²¹)nm³/mL*3/4/pi)^(1/3)*2							
8	Factor = Bubble diameter/Droplet Diameter							
9								
10	PFC	Boiling point (°C)	Liquid Density (g/mL)	Molecular weight (g/mol)	n (mol)	Vbubble (L)	Bubble Diameter (nm)	Factor
11	PFH	56.6	1.71	338	2.12E-17	5.40E-16	1010.1	5.05
12	PFMP	49.2	1.6	316.04	2.12E-17	5.40E-16	1010.3	5.05
13	PFP	29	1.63	288	2.37E-17	6.04E-16	1048.6	5.24
14	PFB	-1.7	1.594	238.03	2.81E-17	7.14E-16	1109.0	5.55

APPENDIX B: CALCULATIONS FOR ESTIMATED VAPOR TEMPERATURES

Equation 6 shows a modified version of the Antoine equation where the vapor temperature is a function of the droplet radius taking into account the Laplace pressure.

$$T = \frac{B}{A - \log_{10}\left(P_{atm} + P_{body} + \frac{2\sigma}{r}\right)} - C$$

The corresponding spreadsheet setup along with formulas is shown below.

	A	B	C	D	E	F	G	H
1	Patm (bar)	Pbody (bar)		d (nm)	r (m)	Substance	T (K)	T (°C)
2	1.013	0.12		100	5E-08	Perfluorohexane	425.21	152.06
3				102	5.1E-08	A	424.27	151.12
4	surface tension (N/M)			104	5.2E-08	4.07362	423.35	150.20
5	51			106	5.3E-08	B	422.46	149.31
6				108	5.4E-08	1113.329	421.59	148.44
7	r = d/2/(10^9)			110	5.5E-08	C	420.74	147.59
8				112	5.6E-08	-56.472	419.91	146.76
9	T(K) = B/(A-			114	5.7E-08		419.10	145.95
10	LOG(Patm+Pbody+σ/r/1000*(10^-5),10))-			116	5.8E-08	Temperature (K)	418.31	145.16
11	C			118	5.9E-08	256.43-447.08	417.54	144.39
12				120	6E-08		416.79	143.64
13	T (°C) = T(K) - 273.15			122	6.1E-08		416.05	142.90
14				124	6.2E-08		415.33	142.18
15				126	6.3E-08		414.63	141.48
16				128	6.4E-08		413.94	140.79
17				130	6.5E-08		413.26	140.11
18				132	6.6E-08		412.60	139.45
19				134	6.7E-08		411.96	138.81
20				136	6.8E-08		411.32	138.17
21				138	6.9E-08		410.70	137.55
22				140	7E-08		410.09	136.94
23				142	7.1E-08		409.50	136.35
24				144	7.2E-08		408.91	135.76
25				146	7.3E-08		408.33	135.18
26				148	7.4E-08		407.77	134.62
27				150	7.5E-08		407.22	134.07
28				152	7.6E-08		406.67	133.52
29				154	7.7E-08		406.14	132.99

◇	I	J	K	L	M	N	O
1	Substance	T (K)	T (°C)		Substance	T (K)	T (°C)
2	Perfluoropentane	390.94914	117.79914		Perfluorobutane	351.80297	78.652966
3	A	390.07403	116.92403		A	351.00824	77.858242
4	4.38423	389.22154	116.07154		4.1425	350.23434	77.084338
5	B	388.39069	115.24069		B	349.48033	76.330335
6	1257.758	387.58053	114.43053		982.586	348.74537	75.595367
7	C	386.79021	113.64021		C	348.02863	74.878625
8	-13.231	386.01889	112.86889		-33.624	347.32935	74.179347
9		385.2658	112.1158			346.64681	73.496814
10	Temperature (K)	384.53022	111.38022		Temperature (K)	345.98035	72.830352
11	300-421.8	383.81146	110.66146		233.27-269.24	345.32932	72.179323
12		383.10886	109.95886			344.69312	71.543124
13		382.42182	109.27182			344.07119	70.921188
14		381.74975	108.59975			343.46297	70.312975
15		381.0921	107.9421			342.86798	69.717977
16		380.44834	107.29834			342.28571	69.13571
17		379.818	106.668			341.71572	68.565716
18		379.20058	106.05058			341.15756	68.007561
19		378.59565	105.44565			340.61083	67.460832
20		378.00278	104.85278			340.07514	66.925135
21		377.42157	104.27157			339.5501	66.400098
22		376.85162	103.70162			339.03536	65.885363
23		376.29258	103.14258			338.53059	65.380593
24		375.74409	102.59409			338.03546	64.885462
25		375.20582	102.05582			337.54966	64.399664
26		374.67744	101.52744			337.0729	63.922903
27		374.15865	101.00865			336.6049	63.454897
28		373.64917	100.49917			336.14538	62.995378
29		373.1487	99.998701			335.69409	62.544088

◇	P	Q	R	S	T	U
1		Substance	T (K)	T (°C)		
2		Perfluoropropane	307.72678	34.576778		
3		A	307.02085	33.870851		
4		4.08856	306.33348	33.183478		
5		B	305.66384	32.513836		
6		842.613	305.01116	31.861156		
7		C	304.37471	31.224712		
8		-30.023	303.75382	30.603824		
9			303.14785	29.997852		
10		Temperature (K)	302.55619	29.406192		
11		193.78-236.81	301.97828	28.828275		
12			301.41356	28.263564		
13			300.86155	27.711551		
14			300.32176	27.171757		
15			299.79373	26.643725		
16			299.27703	26.127026		
17			298.77125	25.621251		
18			298.27601	25.126012		
19			297.79094	24.640941		
20			297.31569	24.165687		
21			296.84992	23.699916		
22			296.39331	23.243313		
23			295.94557	22.795573		
24			295.50641	22.356409		
25			295.07555	21.925546		
26			294.65272	21.502721		
27			294.23768	21.087682		
28			293.83019	20.680191		
29			293.43002	20.280017		

APPENDIX C: DATA AND DATA ANALYSIS FOR STABILITY

Below are tables showing the z-averages of droplets for different storage temperatures over a period of 16-weeks. Z-averages of each sample were compared to baseline values at week 0 where the baseline values were taken as the “stable values” for error analysis. All samples were acquired using a 200 nm membrane filter. Asterisks indicate measurements were attempted but could not be measured due to technical reasons, and dashes indicate measurements were not attempted. Double dashes indicate mean was not calculated.

Temperature = 4°C		Week					
Perfluorocarbon	Sample	0	2	4	8	12	16
PFH	1	246.00	222.40	244.30	216.40	236.20	245.30
	2	218.80	200.60	202.30	199.20	193.10	200.40
	3	199.80	190.40	189.10	183.30	183.70	190.50
mean		221.53	204.47	211.90	199.63	204.33	212.07
PFMP	4	240.10	231.20	230.60	230.70	229.00	244.30
	5	153.20	153.20	151.60	157.70	151.40	156.70
	6	280.20	259.60	260.30	263.00	261.80	270.60
mean		224.50	214.67	214.17	217.13	214.07	223.87
PFP	7	156.40	157.70	156.70	155.40	153.70	156.70
	8	253.00	232.30	244.40	228.90	233.80	235.40
	9	215.00	206.90	200.40	201.20	211.00	215.90
mean		208.13	198.97	200.50	195.17	199.50	202.67

Temperature = 23°C		Week					
Perfluorocarbon	Sample	0	2	4	8	12	16
PFH	1	189.10	184.90	182.20	197.30	222.30	283.40
	2	249.70	235.20	166.00	205.30	195.70	162.70
	3	192.20	211.40	204.70	182.20	203.40	172.20
mean		210.33	210.50	184.30	194.93	207.13	206.10
PFMP	4	341.50	204.50	201.70	170.40	196.70	185.20
	5	219.40	394.80	373.50	323.40	*	*
	6	219.40	200.90	194.00	190.60	209.40	191.70
mean		260.10	266.73	256.40	228.13	--	--
PFP	7	255.80	209.20	234.00	214.50	269.20	289.20
	8	553.80	617.50	900.30	564.90	796.50	*
	9	172.70	188.60	238.70	184.40	332.10	*
mean		327.43	338.43	457.67	321.27	465.93	--

Temperature = 40°C		Week					
Perfluorocarbon	Sample	0	2	4	8	12	16
PFH	1	467.10	32.02	33.27	37.13	62.81	-
	2	233.20	82.73	37.91	48.81	58.84	-
	3	156.90	113.40	39.90	49.11	44.30	-
mean		285.73	76.05	37.03	45.02	55.32	-
PFMP	4	191.70	106.40	44.19	40.05	42.41	-
	5	147.30	109.50	40.77	39.77	*	-
	6	164.10	107.70	39.59	49.85	79.64	-
mean		167.70	107.87	41.52	43.22	--	-
PFP	7	186.70	108.70	39.35	36.25	*	-
	8	203.80	156.60	133.90	131.10	57.85	-
	9	138.70	41.83	41.07	34.12	*	-
mean		176.40	102.38	71.44	67.16	--	-

The stability of a droplet was determined based upon how well the sample of droplets remained the same size in terms of z-average and if their deviation was less than 10 percent from the baseline z-average. Percent deviations were calculated for each individual sample then averaged for each corresponding perfluorocarbon and week. Bolded numbers in the following tables indicate average percent deviation greater than 10 percent. In other words, the percent deviation was calculated as a standard error shown in the following equation.

$$\text{percent deviation} = \frac{z\text{-average}_{\text{week } n} - z\text{-average}_{\text{baseline}}}{z\text{-average}_{\text{baseline}}} \times 100\% \quad \text{Equation C1}$$

The error bars were calculated as the standard deviations from the sample sets.

AVERAGE PERCENT DEVIATION RELATIVE TO WEEK 0					
Temperature = 4°C					
PFC	Week				
	2	4	8	12	16
PFH	-7.54	-4.53	-9.75	-7.93	-4.45
PFMP	-3.69	-4.03	-2.37	-4.12	0.20
PFP	-3.71	-3.33	-5.53	-3.73	-2.12

Temperature = 23°C					
PFC	Week				
	2	4	8	12	16
PFH	0.65	-10.22	-6.22	0.59	1.54
PFMP	10.47	5.91	-5.28	-	-
PFP	0.83	30.75	-2.46	47.12	-

Temperature = 40°C					
PFC	Week				
	2	4	8	12	16
PFH	-61.80	-83.73	-79.94	-77.70	-
PFMP	-34.84	-75.05	-73.91	-	-
PFP	-44.93	-61.20	-63.89	-	-

One-way analysis of variance (ANOVA) was performed via StatPlus for each sample set. Below are the results from the ANOVA tests performed.

4°C						
Summary						
<i>Groups</i>	<i>Sample size</i>	<i>Sum</i>	<i>Mean</i>	<i>Variance</i>		
<i>PFH</i>	5	-34.2	-6.84	5.2986		
<i>PFMP</i>	5	- 14.01	-2.802	3.30807		
<i>PFP</i>	5	- 18.42	-3.684	1.49548		
ANOVA						
<i>Source of Variation</i>	<i>SS</i>	<i>df</i>	<i>MS</i>	<i>F</i>	<i>p-level</i>	<i>F crit</i>
Between Groups	45.07284	2	22.53642	6.69256	0.01116	5.5163
Within Groups	40.4086	12	3.36738			
<i>Total</i>	85.48144	14				

23°C						
Summary						
<i>Groups</i>	<i>Sample size</i>	<i>Sum</i>	<i>Mean</i>	<i>Variance</i>		
<i>PFH</i>	5	-13.66	-2.732	27.23997		
<i>PFMP</i>	3	11.1	3.7	65.6787		
<i>PFP</i>	4	76.24	19.06	573.15433		
ANOVA						
<i>Source of Variation</i>	<i>SS</i>	<i>df</i>	<i>MS</i>	<i>F</i>	<i>p-level</i>	<i>F crit</i>
Between Groups	1,079.12832	2	539.56416	2.47787	0.1389	6.234
Within Groups	1,959.78028	9	217.75336			
<i>Total</i>	3,038.9086	11				

40°C						
Summary						
<i>Groups</i>	<i>Sample size</i>	<i>Sum</i>	<i>Mean</i>	<i>Variance</i>		
<i>PFH</i>	4	-303.17	-75.7925	93.21143		
<i>PFMP</i>	3	-183.8	-61.26667	524.10143		
<i>PFP</i>	3	-170.02	-56.67333	105.23843		
ANOVA						
<i>Source of Variation</i>	<i>SS</i>	<i>df</i>	<i>MS</i>	<i>F</i>	<i>p-level</i>	<i>F crit</i>
Between Groups	710.83968	2	355.41984	1.61732	0.2646	7.20257
Within Groups	1,538.31401	7	219.75914			
<i>Total</i>	2,249.15369	9				

APPENDIX D: SEM IMAGE OF PFP DROPLETS

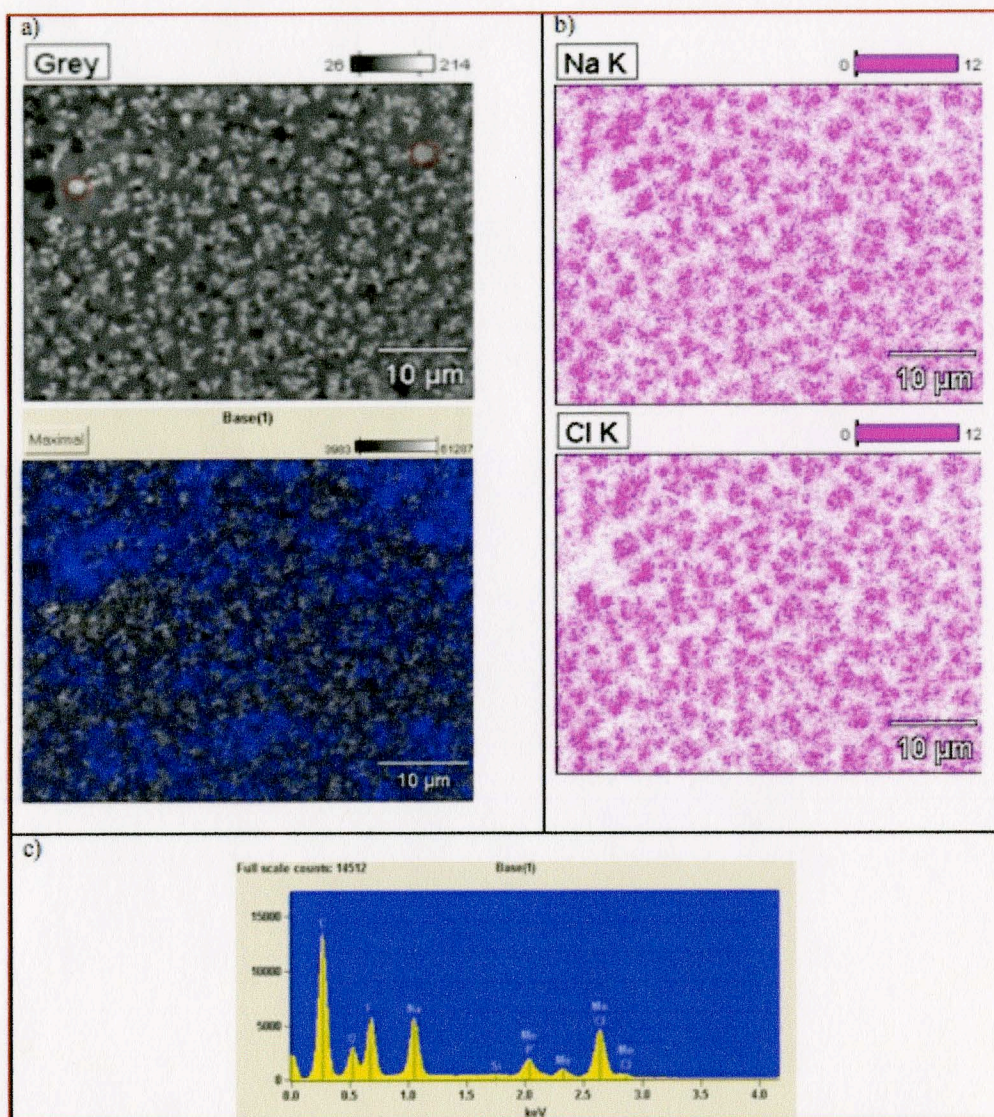


Figure D1. Perfluoropentane droplet sample. a) SEM image and corresponding EDS of fluorine detected. Red circles in grey image indicate potential PFP droplets. b) Na and Cl EDS detected indicating potential salt crystal structures. c) EDS spectra obtained when analyzing perfluoropentane droplet sample.

REFERENCES

- Alkan-Onyuksel H, Demos SM, Lanza GM, Vonesh MJ, Klegerman ME, Kane BJ, Kuszak J, McPherson DD. Development of inherently echogenic liposomes as an ultrasonic contrast agent. *Journal of Pharmaceutical Sciences* 1996; 85:486–490.
- Altekruse SF, Kosary CL, Krapcho M, Neyman N, Aminou R, Waldron W, Ruhl J, Howlander N, Tatalovich Z, Cho H, Mariotto A, Eisner MP, Lewis DR, Cronin K, Chen HS, Feuer EJ, Stinchcomb DG, Edwards BK (eds). SEER Cancer Statistics Review, 1975-2007, National Cancer Institute. Bethesda, MD, http://seer.cancer.gov/csr/1975_2007/, based on November 2009 SEER data submission, posted to the SEER web site, 2010. Accessed 8 July 2010.
- Bamett SB, Walsh DA, Angles JA. Novel approach to evaluate the interaction of pulsed ultrasound with embryonic development. *Ultrasonics* 1990; 28:166- 170.
- Barnett SB, Rott HD, Ter Haar GR, Ziskin MC, Maeda K. The sensitivity of biological tissue to ultrasound. *Ultrasound in Medicine & Biology* 1997; 23:805–812.
- Barnett SB, Ter Haar GR, Ziskin MC, Rott HD, Duck FA, Maeda K. International recommendations and guidelines for the safe use of diagnostic ultrasound in medicine. *Ultrasound in Medicine & Biology* 2000; 26:355-66.
- Basude R, Duckworth JW, Wheatley MA. Influence of environmental conditions on a new surfactant-based contrast agent: ST68. *Ultrasound in Medicine & Biology* 2000; 26:621-628.
- Bensley, DM. Drug stability guidelines. Guidance for industry. U.S. Department of Health and Human Services Food and Drug Administration Rockville, MD. <http://www.fda.gov/downloads/AnimalVeterinary/GuidanceComplianceEnforcement/GuidanceforIndustry>, Dec 2008. Accessed 27 May 2011.
- Biro GP, Blais P, Rosen AL. Perfluorocarbon blood substitutes. *Critical Reviews in Oology/Hematology* 1987; 6:311-374.
- Blodgett T. Breast Cancer PET/CT Imaging Protocol. http://www.omillc.com/newsletter/omi_newslsletter_2.10.pdf, PET/CT Newsletter Feb 2010; 7:7. Accessed 23 January 2011.
- Borden MA, Caskey CF, Little E, Gillies RJ, Ferrara KW. DNA and polylysine adsorption and multilayer construction onto cationic lipid-coated microbubbles. *Langmuir* 2007; 23:9401-9408.

- Burgess DJ, Yoon JK. Influence of interfacial properties on perfluorocarbon/aqueous emulsion stability. *Colloids and Surfaces B: Biointerfaces* 1995; 4:297-308.
- Chemical Book, "2H,3H-Decafluoropentane", Copyright 2008a. [Online]. Available: http://www.chemicalbook.com/ProductChemicalPropertiesCB3283226_EN.htm. Accessed 7 April 2011.
- Chemical Book, "Perfluoro-2-methyl-3-pentanone", Copyright 2008b. [Online]. Available: http://www.chemicalbook.com/ProductChemicalPropertiesCB2238274_EN.htm. Accessed 9 June 2010.
- Chetanachan P, Akarachalanon P, Worawirunwong D, Dararutana P, Bangtrakulnonth A, Bunjop M, Kongmuang S. Ultrastructural characterization of liposomes using transmission electron microscope. *Advanced Materials Research* 2008; 55-57:709-711.
- Cohen J, Simons RF, Edwards RG, Fehilly CB, Fishel SB. Pregnancies following the frozen storage of expanding human blastocysts. *Journal of In Vitro Fertilization and Embryo Transfer* 1985; 2:59-64.
- Dayton PA, Zhao S, Bloch SH, Schumann P, Penrose K, Matsunaga TO, Zutshi R, Doinikov A, Ferrara KW. Application of ultrasound to selectively localize nanodroplets for targeted imaging and therapy. *Molecular Imaging* 2006; 5:160-174.
- Fan X, River JN, Muresan AS, Popescu C, Zamora M, Culp RM, Karczmar GS. MRI of perfluorocarbon emulsion kinetics in rodent mammary tumors. *Physics in Medicine and Biology* 2006; 51:211-220.
- Fehilly CB, Cohen J, Simons RF, Fishel SB, Edwards RG. Cryopreservation of cleaving embryos and expanded blastocysts in the human: a comparative study. *Fertility and Sterility* 1985; 44:638-644.
- Forsberg F, Shi WT, Merritt CRB, Dai Q, Solcova M, Goldberg BB. On the usefulness of the mechanical index displayed on clinical ultrasound scanners for predicting contrast microbubble destruction. *Journal of Ultrasound in Medicine* 2005; 24:443-450.
- Gao Z, Kennedy AM, Christensen DA, Rapoport NY. Drug-loaded nano/microbubbles for combining ultrasonography and targeted chemotherapy. *Ultrasonics* 2008; 48:260-270.

- Giesecke T, Hynynen K. Ultrasound-mediated cavitation thresholds of liquid perfluorocarbon droplets *in vitro*. *Ultrasound in Medicine & Biology* 2003; 29:1359-1365.
- Gramiak R, Shah PM. Echocardiography of the aortic root. *Investigative Radiology* 1968; 3:356-366.
- Hobbs SK, Monsky WL, Yuan F, Roberts WG, Griffith L, Torchilin VP, Jain RK. Regulation of transport pathways in tumor vessels: Role of tumor type and microenvironment. *Proceedings of the National Academy of Sciences USA* 1998; 95:4607-4612.
- Holland CK, Apfel RE. Thresholds for transient cavitation produced by pulsed ultrasound in a controlled nuclei environment. *Journal of Acoustical Society of America* 1990; 88:2059-2069.
- Huh D, Bahng JH, Ling Y, Wei HH, Kripfgans OD, Fowlkes JB, Grothberg JB, Takayama S. Gravity-driven microfluidic particle sorting device with hydrodynamic separation amplification. *Analytical Chemistry* 2007; 79:1369-1376.
- Jackson BA, Schwane JA, Starcher BC. Effect of ultrasound therapy on the repair of Achilles tendon injuries in rats. *Medicine and Science in Sports and Exercise* 1991; 2:171-176.
- Jain RK, Duda DG. "Angiogenesis in Solid Tumors." In *Antiangiogenic Cancer Therapy*. Ed. Darren W. Davis, Roy S. Herbst. Boca Raton, FL: CRC Press, 2008. 43-90. Print.
- Janjic JM, Srinivas M, Kadayakkara DKK, Ahrens ET. Self-delivering nanoemulsions for dual fluorine-19 MRI and fluorescence detection. *Journal of the American Chemical Society* 2008; 130:2832-2841.
- Kawabata K, Sugita N, Yoshikawa H, Azuma T, Umemura S. Nanoparticles with multiple perfluorocarbons for controllable ultrasonically induced phase shifting. *Japanese Journal of Applied Physics* 2005; 44:4548:4552.
- Kiepert PE. Perfluorocarbon emulsions: future alternatives to transfusion. *Blood Substitutes: Principles, Methods, Products and Clinical Trials* 1998; 2:127-156.
- Kripfgans OD, Fowlkes JB, Miller DL, Eldevik OP, Carson PL. Acoustic droplet vaporization for therapeutic and diagnostic applications. *Ultrasound in Medicine & Biology* 2000; 26:1177-1189.

- Kripfgans OD, Fowlkes JB, Woydt M, Eldevik OP, Carson PL. In vivo droplet vaporization for occlusion therapy and phase aberration correction. *IEEE Transactions on Ultrasonics, Ferroelectrics and Frequency Control* 2002; 49:726-738.
- Lide DR ed., *CRC Handbook of Chemistry and Physics*, 90th Edition (Internet Version 2010), CRC Press/Taylor and Francis, Boca Raton, FL. <<http://www.hbcpnetbase.com/>>. Accessed 9 July 2010.
- Linstrom PJ, Mallard WG, Eds., *NIST Chemistry WebBook*, NIST Standard Reference Database Number 69, National Institute of Standards and Technology, Gaithersburg MD, 20899, <<http://webbook.nist.gov>>. Accessed 19 September 2010.
- Lo AH, Kripfgans OD, Carson PL, Rothman ED, Fowlkes JB. Acoustic droplet vaporization threshold: effects of pulse duration and contrast agent. *IEEE Transactions on Ultrasonics, Ferroelectrics and Frequency Control* 2007; 54:933-46.
- Maeda H, Noguchi Y, Sato K, Akaike T. Enhanced vascular permeability in solid tumor is mediated by nitric oxide and inhibited by both new nitric oxide scavenger and nitric oxide synthase inhibitor. *Japanese Journal of Cancer Research* 1994; 85:331-334.
- Massoud TF, Gambhir SS. Molecular imaging in living subjects: seeing fundamental biological processes in a new light. *Gene & Development* 2003; 17:545-580.
- Matsumura Y, Maeda H. A new concept for macromolecular therapeutics in cancer chemotherapy: mechanism of tumoritropic accumulation of proteins and the antitumor agent Smancs. *Cancer Research* 1986; 46:6387-6392.
- McClements DJ. "Context and Background." In *Food Emulsions: Principles, Practices, and Techniques*. 2nd Ed. Boca Raton, FL: CRC Press, 2005. 1-26. Print.
- Mayer LD, Krishna R, Bally MB. Liposomes for Cancer Therapy Applications. In *Polymeric Biomaterials*. Ed. Severian Dumitriu. New York: Marcel Dekker, 2002. 823-841. Print.
- Nam KH, Christensen DA, Kennedy AM, Rapoport N. Acoustic droplet vaporization, cavitation, and therapeutic properties of copolymer-stabilized perfluorocarbon nanoemulsions. *AIP Conference Proceedings* 2009; 1113:124-128.

- Narang U, Dunbar RA, Bright FV, Prasad PN. Chemical sensor based on an artificial receptor element trapped in a porous sol-gel glass matrix. *Applied Spectroscopy* 1993; 47:1700-1703.
- Pan LK, Wang CKC. Superheated-liquid-droplet technique for measuring alpha decays in uranium solutions. *Nuclear Instruments and Methods in Physics Research A* 1999; 420:345-355.
- Prince JL, Links JM. "Ultrasound Imaging." In *Medical Imaging Signals and Systems*. Upper Saddle River: Pearson Education, 2006. 313-378. Print.
- Porter TR, Xie F. Visually discernible myocardial echocardiographic contrast after intravenous injection of sonicated dextrose albumin microbubbles containing high molecular weight, less soluble gases. *Journal of the American College of Cardiology* 1995; 25: 509-515.
- Rapoport N, Gao Z, Kennedy A. Drug-loaded nanoemulsions/microbubbles for combined tumor imaging and therapy. 6th International Symposium on Therapeutic Ultrasound 2007; 472-478.
- Rapoport NY, Efros AL, Christensen DA, Kennedy AM, Nam KH. Microbubble generation in phase-shift nanoemulsions used as anticancer drug carriers. *Bubble Science, Engineering and Technology* 2009; 1(1-2): 31-39.
- Schad KC, Hynynen K. *In vitro* characterization of perfluorocarbon droplets for focused ultrasound therapy. *Physics in Medicine and Biology* 2010; 55:4933-4947.
- Skyba DM, Price RJ, Linka AZ, Skalak TC, Kaul S. Direct in vivo visualization of intravascular destruction of microbubbles by ultrasound and its local effects on tissue. *Circulation* 1998; 28:290-293.
- Sheeran PS, Wong VP, McFarland RJ, Ross W, Feingold SJ, Matsunaga TO, Dayton PA. Decafluorobutane as a phase-change contrast agent for low-energy extravascular ultrasound imaging. *Ultrasound in Medicine & Biology* 2011; 6:PP?.
- Singhal S, Moser CC, Wheatley MA. Surfactant-stabilized microbubbles as ultrasound contrast agents: stability study of Span 60 and Tween 80 mixtures using a Langmuir trough. *Langmuir* 1996; 9:2426-2429.
- Song J, Qi M, Kaul S, Price RJ. Stimulation of arteriogenesis in skeletal muscle by microbubble destruction with ultrasound. *Circulation* 2002; 17;106:1550- 1555.

- Song J, Cottler PS, Klibanov AL, Kaul S, Price RJ. Microvascular remodeling and accelerated hyperemia blood flow restoration in arterially occluded skeletal muscle exposed to ultrasonic microbubble destruction. *American Journal of Physiology – Heart and Circulatory Physiology* 2004; 287:2754-2761.
- Spahn DR, Leone BJ, Reves JG, Pasch T. Cardiovascular and coronary physiology of acute isovolemic hemodilution: a review of nonoxygen-carrying and oxygen carrying solutions. *Anesthesia & Analgesia* 1994; 78:1000-1021.
- Speed CA. Therapeutic ultrasound in soft tissue lesions. *Rheumatology* 2001; 12:1331-1336.
- Sticker TP, Kumar V. "Neoplasia." In *Robbins Basic Pathology*. Ed. Vinay Kumar, Abul K. Abbas, Nelson Fausto, Richard N. Mitchell. Philadelphia, PA: Saunders/Elsevier, 2007. 172-223. Print.
- Thomsen HS. "Radiography with gadolinium contrast agents." In *Contrast media: safety issues and ESUR guidelines*. Ed. HS Thomsen, JAW Webb. Berlin; Heidelberg: Springer, 2009. 171-177. Print.
- Unger E, Matsunaga TO, Schumann PA, Zutshi R. Microbubbles in molecular imaging and therapy. *MedicaMundi* 2003; 47: 58-65.
- Vaupal P, Kallinowski F, Okunieff P. Blood flow, oxygen and nutrient supply, and metabolic microenvironment of human tumors: A review. *Cancer Research* 1989; 49:6449-6465.
- Walsh DA, Klein NW, Hightower LE, Edwards MJ. Heat shock and thermotolerance during early rat embryo development. *Teratology* 1987;36:181-191.
- Wang CK, Lim W, Pan LK. Use of superheated liquid dispersion technique for measuring alpha-emitting actinides in environmental samples. *Nuclear Instruments and Methods in Physics Research A* 1994; 353:524-527.
- Waters EA, Chen J, Allen JS, Zhang H, Lanza GM, Wickline SA. Detection and quantification of angiogenesis in experimental valve disease with integrin targeted nanoparticles and 19-fluorine MRI/MRS. *Journal of Cardiovascular Magnetic Resonance* 2008; 10:43-51.
- Wei K, Jayaweera AR, Firoozan S, Linka A, Skyba DM, Kaul S. Quantification of myocardial blood flow with ultrasound-induced destruction of microbubbles administered as a constant venous infusion. *Circulation* 1998; 97:473-483.

Ziskin MC. Intrauterine effects of ultrasound: human epidemiology. *Teratology* 1999; 59:252-260.